THE ASTROPHYSICAL JOURNAL, 348:542–556, 1990 January 10

OBSERVATIONS OF THE FORMALDEHYDE EMISSION IN ORION-KL: ABUNDANCES, DISTRIBUTION, AND KINEMATICS OF THE DENSE GAS IN THE ORION MOLECULAR RIDGE

JEFFREY G. MANGUM,[1,2,3] ALWYN WOOTTEN,[2] ROBERT B. LOREN,[4] AND E. JAMES WADIAK[2]
Received 1989 January 9; accepted 1989 July 8

ABSTRACT

The "hot core," "plateau," and "ridge" features in the Orion-KL molecular cloud have been mapped in 2 cm H_2CO emission with a 6″ synthesized beam. We have also observed all $\Delta J = 1$ millimeter wave transitions of H_2CO and several of the $H_2{}^{13}CO$ and $H_2C^{18}O$ transitions in the 211 to 363 GHz window toward Orion-KL with a single antenna. The H_2CO hot core emission has been identified for the first time both in high-excitation line profiles and in the 2 cm maps. We identify a velocity shift in the 2 cm H_2CO emission which we attribute to the plateau or bipolar flow. This velocity shift lies at a position angle of $120° \pm 30°$, which is parallel to the bipolar flows seen in SiO, HCO^+, H_2, SO_2, CO, and SO emission. The large primary beam available for these observations has provided a particularly sensitive map of the rather extended "ridge" structure in Orion-KL. The "ridge" component in our 2 cm H_2CO emission maps can be decomposed into two clumps, called the "compact ridge" and "10 km s^{-1} feature." The compact ridge dominates the observed emission. Comparison with aperture synthesis maps in other molecules demonstrates that the 2 cm H_2CO compact ridge defines an extensive high-density ($\gtrsim 10^6$ cm^{-3}) region at the southern edge of the bipolar flow near IRc2.

With this multitransition, multi-isotopomer[5] data set, we have modeled the spatial density in the compact ridge component. We find that $n(H_2) = 5.0 \times 10^6$–1.0×10^7 cm^{-3} in the H_2CO compact ridge. These models also reveal that there is no evidence for substantial variation in the H_2CO abundances among the hot core, compact ridge, and 10 km s^{-1} feature. However, H_2CO is 3–25 times more abundant in these Orion-KL components than it is in other molecular clouds (Mundy *et al.*; Wootten *et al.*). This abundance enhancement may be due to the epidemic of massive star formation in the region. Observers have noted in the past that 2 cm H_2CO emission occurs only rarely in interstellar clouds, though density sufficient to cause the emission is found in many cloud cores. We suggest that the reason the emission is notably intense in Orion-KL lies in the enhancement of the H_2CO abundance, as well as in the high density.

Subject headings: interstellar: molecules — nebulae: abundances — nebulae: individual (Orion Nebula)

I. INTRODUCTION

The formaldehyde (H_2CO) molecule, ubiquitous in the interstellar medium, emits strongly at many wavelengths, making it a useful probe of molecular cloud conditions, such as density or temperature. Frequently, H_2CO is employed to probe the density in interstellar clouds. Collisional pumping of the molecule can produce excitation temperatures below 2.7 K in the $J_{K-1K_1} = 1_{10} \rightarrow 1_{11}$ and $2_{11} \rightarrow 2_{12}$ transitions, causing them to be observed most often in absorption against the microwave background. Densities above 10^6 cm^{-3} quench this collisional pump, causing the lines to then appear in emission. Of the six known regions in the sky where the $2_{11} \rightarrow 2_{12}$ transition is seen in emission, the Orion molecular cloud (OMC-1 or Orion-KL) core has attracted the most scrutiny. Theoretically, formaldehyde's chemical sensitivity to temperature could justify its use as a thermal tracer of the chemistry in a region. On Earth, it is produced as methane is oxidized into CO_2. However, the key reactions with O, OH, and H which destroy H_2CO, and lead to the creation of CO and CO_2, require energy too substantial for most interstellar environments (Wootten, Loren, and Bally 1984). In these cool clouds, the oxidation path is blocked and the H_2CO abundance is high, whereas on Earth its abundance is low. As a thermometer, then, H_2CO should discriminate between warm and hot (i.e., Earth-like temperature) chemistries.

It is somewhat surprising, then, that H_2CO emission arises from the "plateau" ($V_{LSR} \simeq 8$ km s^{-1}, $\Delta V \gtrsim 20$ km s^{-1}, $T_K \simeq$ 100 K; for a detailed summary of all of the Orion-KL emission component parameters, see Blake *et al.* 1987) component in Orion-KL, as this material is thought to have been accelerated by shocks, and hence processed through very warm regions where H_2CO might have been destroyed (Wootten, Loren, and Bally 1984). Single-antenna maps of the Orion-KL region in the $2_{11} \rightarrow 2_{12}$ transition (Bastien *et al.* 1985) confirmed the presence of two distinct profile components identified by single-antenna observers as the unresolved "plateau" and "ridge" (Johansson *et al.* 1984; Olofsson 1984; Wootten, Loren, and Bally 1984) components. This weak "plateau" component, more strongly identified in CO, SiO, HCO^+, SO_2, and H_2 emission maps, probably originates in a bipolar flow emanating from IRc2 (Masson *et al.* 1987; Wright *et al.* 1983; Vogel *et al.* 1984; Plambeck 1987; Hough *et al.* 1986). It seems

[1] Department of Astronomy, University of Virginia, Charlottesville, Virginia.
[2] National Radio Astronomy Observatory, Charlottesville, Virginia.
[3] National Radio Astronomy Observatory Junior Research Associate.
[4] Millimeter Wave Observatory, Electrical Engineering Research Laboratory, and Department of Astronomy, the University of Texas at Austin.
[5] In this context, the term "isotopomer" is more appropriate than the more commonly used term, "isotope." The term "isotope" refers to atoms of the same chemical element that have the same atomic number but differ in atomic mass. "Isotopomer," constructed from the Greek ισο, meaning equal, τοποσ, meaning place, and μερος, meaning part or share, is a more appropriate usage for molecular species.

that the dynamics and spatial structure of the "plateau" region conspire to create an environment favorable to the survival of H_2CO, but the structure of the "plateau" region has remained unresolved. The "ridge" component, however, can be resolved in the Bastien *et al.* maps into two clumps, called the "compact ridge" ($V_{LSR} \simeq 8$ km s^{-1}, $\Delta V \simeq 4.0$ km s^{-1}, $T_K \simeq 95$ K) and "10 km s^{-1} feature" ($V_{LSR} \simeq 10$ km s^{-1}, $\Delta V \simeq 1.0$ km s^{-1}, $T_K \simeq 55$ K). The spatial structure of the H_2CO emitting region remained poorly known, however, so we have made aperture synthesis maps of emission in the $2_{11} \rightarrow 2_{12}$ line of H_2CO in Orion-KL, which we present in this paper.

Transitions in the $K = 2$ and $K = 3$ ladders of H_2CO have received little attention from observers because they lie at relatively high frequencies. However, these transitions are difficult to excite and therefore can highlight hot, dense regions. The archetype of such regions is the "hot core" ($V_{LSR} \simeq 6$ km s^{-1}, $\Delta V \simeq 10$ km s^{-1}, $T_K \simeq 150$–275 K) of Orion-KL, which we identify for the first time as a distinct velocity and temperature component in the profiles of lines in the $K = 2$ and $K = 3$ ladders of H_2CO. Interferometer maps, with their sensitivity to high spatial frequencies, locate $2_{11} \rightarrow 2_{12}$ H_2CO emission coinciding in position and extent with the "hot core" measured in other molecules. This confirms the existence of H_2CO in the hot core, previously suspected only from the asymmetry of the single-antenna line profiles. New single-antenna observations of 14 H_2CO, eight $H_2{}^{13}CO$, and four $H_2C^{18}O$ transitions lying between 211 and 363 GHz further detail the characteristics of the various emitting regions. We have modeled this multitransition, multi-isotopomer data set in conjunction with our high-resolution interferometric observations to study the physical conditions in the compact ridge component.

Spectral surveys of this region (Blake *et al.* 1987; Johansson *et al.* 1984) have described the striking physical and chemical distinctions between these four distinct velocity features. These single-antenna surveys, though, do not reveal how the various velocity components are related dynamically. Our aperture synthesis observations have enabled us to study the dynamical interactions between the four velocity components.

II. OBSERVATIONS

a) Interferometric

Observations of the $2_{11} \rightarrow 2_{12}$ transition of H_2CO (rest frequency 14.488479 GHz) were made on 1987 March 1 using the NRAO Very Large Array[6] in the D-configuration with 24 operational antennas. The total observing bandwidth of 3.125 MHz was divided into 128 spectral line channels, with only the inner 31 channels retained. On-line Hanning smoothing was employed, yielding a frequency resolution and channel spacing of 24.4 kHz, or 0.5 km s^{-1} at the line rest frequency. Although the $2_{11} \rightarrow 2_{12}$ line consists of several hyperfine components, they lie too closely spaced in frequency to be resolved in the broad-lined Orion-KL source. The nominal observing frequency was readjusted every 20 minutes to maintain a center channel LSR velocity of 9.0 ± 0.05 km s^{-1}, with total velocity coverage of $0.9 \leq V_{LSR} \leq 17.1$ km s^{-1}. The flux density scale was established by observing 3C 286 (assumed flux density 3.53 Jy) for 10 minutes at the end of the 4 hr observing run. Orion-KL was observed at an antenna pointing and phase center position of $\alpha(1950) = 05^h32^m47^s.0$, $\delta(1950) = -05°24'17''$ for 14 minute periods alternated with 6 minute observations of the calibration source 0529+075 (measured flux density 1.45 Jy).

The antenna amplitudes and phases were calibrated in the normal manner using 0529+075, which was also used to calibrate the spectral bandpass response. Maps of each spectral line channel were made using a cell size of 1".5 with natural weighting and no tapering of the *u-v* plane data. The resulting synthesized beam size for both the line and continumm maps was 6".4 × 5".1, p.a. −14°.3. No correction was made for primary beam taper (3'.5 FWHM) across the field of view in either the line or continuum maps. A line-free continuum map was formed by averaging the six off-line channels at $V_{LSR} > 14$ km s^{-1} which showed no noticeable line emission (although these channels may contain some weak plateau emission). The peak flux and rms noise in this map are 241.4 mJy per beam and 15.3 mJy per beam, respectively. This continuum map was subtracted from each of the un-CLEANed spectral line channel maps. A total of 25 spectral line channels were found to contain line emission. These channels were CLEANed in the normal manner. The typical rms noise in a single channel CLEANed map was 8.9 mJy per CLEAN beam area, corresponding to a main beam brightness temperature of 1.6 K. Comparison with the single dish profiles of Bastien *et al.* (1985) and Vanden Bout (1987) reveal that we have recovered substantially all of the single dish flux.

For better representation of extended structures we tried two alternate reduction techniques. The first was to apply a Gaussian taper of 15 kλ before mapping. After continuum subtraction and CLEANing in the same manner as in the above, we found no evidence for extended structure in our maps. The second was to apply the maximum entropy method of image construction. This, again, yielded no significant changes to our original reduction results.

b) Single Antenna

Observations of 14 transitions of H_2CO (all of the $\Delta J = 1$ transitions lying between 211 and 363 GHz), eight transitions of $H_2{}^{13}CO$, and four transitions of $H_2C^{18}O$ were obtained at various times with the 4.9 m antenna of the Millimeter Wave Observatory (MWO),[7] located near Fort Davis, TX. The pointing center position used in these observations was $\alpha(1950) = 05^h32^m46^s.7$, $\delta(1950) = -05°24'25''$. The receiver was a cooled heterodyne mixer receiver with quasi-optical signal injection developed by N. Erickson (1981). The spectrometer consisted of 128 or 256 channels of 250 kHz filters. The single-sideband system temperature varied from 3000 K at 218 GHz to 25,000 K at 362 GHz (a portion of the steepening system temperature at high frequencies is the result of the much higher atmospheric opacity at the edge of the atmospheric window). At 300 GHz the half-power beam width was measured to be 65". Atmospheric opacity was measured frequently; at the higher frequencies it was typically 0.5. Calibration of the data was effected by synchronous detection of an ambient temperature absorber and the sky.

The intensity of the lines at the MWO must be corrected for the forward scattering and spillover efficiency, η_{fss}, and for the coupling efficiency, η_c, of the antenna diffraction pattern to the source distribution. The true radiation temperature of the

[6] The NRAO is operated by Associated Universities, Inc., under cooperative agreement with the National Science Foundation.

[7] The Millimeter Wave Observatory (MWO) is operated by the Electrical Engineering Research Laboratory, the University of Texas at Austin, with support from the National Science Foundation and the McDonald Observatory.

source is then given by $T_R = T_A^*/\eta_{fss}\eta_c$. A study of the MWO antenna beam at 1.3 mm (Mundy 1981) indicates $\eta_{fss} = 0.83 \pm 0.025$ for frequencies from 211 to 267 GHz. Subsequently, an error-correcting secondary developed by John Davis and Charles Mayer was installed on the antenna, greatly improving its high-frequency performance. Although η_{fss} did not substantially change, the aperture efficiency increased by a factor of 4 and the beam efficiency by a factor of 2. Formaldehyde lines near 290 GHz, whose excitation requirements span a wide range of physical conditions, were found to be stronger by a factor of 1.35 ± 0.1 in Orion-KL, consistent with a source size of $\sim 80''$ by less than $20''$ measured from our map at 300 GHz. Where it has been necessary to compare data taken with different efficiencies, this adjustment has been applied to the older data. Estimation of physical source parameters frequently requires knowledge of T_R. As Jupiter was observed during all observing sessions, $\eta_{fss}\eta_c$ was calculated directly from measurements of T_A^*(Jupiter), assuming T_R(Jupiter) = 160 K. Before installation of the error-corrector, $\eta_{fss}\eta_c = 0.06$ for Jupiter, and after $\eta_{fss}\eta_c = 0.17$, with only a small variation from 215 to 345 GHz. Comparison of the effects of the error-corrector on the relative temperatures of Jupiter and the Orion-KL formaldehyde lines suggests that use of $\eta_{fss}\eta_c = 0.17$ overestimates T_R, but not by more than a factor of 2.

During the 1988 January observations, a faulty A/D converter board caused mismeasurement of the amplitude in every 16th channel in several of our spectra. Therefore, in a few of our spectra we have had to interpolate several channels. We do not feel, though, that this problem has significantly affected our results.

III. RESULTS

a) Interferometric

In the following sections we present the results from our interferometric observations of the H_2CO hot core, plateau, compact ridge, and 10 km s^{-1} feature in Orion-KL. Due to the spatial superposition of the hot core, plateau, and compact ridge, these components are distinguishable mainly through measurement of their central velocities and velocity widths. This spatial superposition is apparent in Figure 1, which is the integrated $2_{11} \rightarrow 2_{12}$ spectral line intensity map. In this map, only the 10 km s^{-1} feature (the secondary peak located to the northeast of the main emission region) is separable from the overall emission distribution.

i) *Hot Core*

In Figures 2 and 3 we present maps of the 2 cm H_2CO hot core component. Figure 2 is an integrated intensity map of the low ($V_{LSR} \leq 6$ km s^{-1}) velocity H_2CO channel maps. Because of the limited velocity coverage of our observations, we were unable to detect all of the low-velocity gas ($V_{LSR} \leq 1$ km s^{-1}). Barvainis and Wootten (1987) observed the $2_{11} \rightarrow 2_{12}$ transition in Orion-KL in a single broad continuum channel, detecting the strongest H_2CO emission near the position of IRc2. Only $\sim 20\%$ of the total integrated emission in our maps comes from this component, however. Therefore we present in Figure 3 the sum of our high ($V_{LSR} \geq 10$ km s^{-1}) and low ($V_{LSR} \leq 6$ km s^{-1}) velocity channel maps. We believe that this map represents a portion of the hot core emission because of its spatial coincidence with other molecular line (Genzel *et al.* 1982; Masson *et al.* 1987; Masson and Mundy 1988; Mundy *et al.* 1988; Plambeck and Wright 1987, 1988) and continuum (Wright and Vogel 1985) hot core features and its velocity

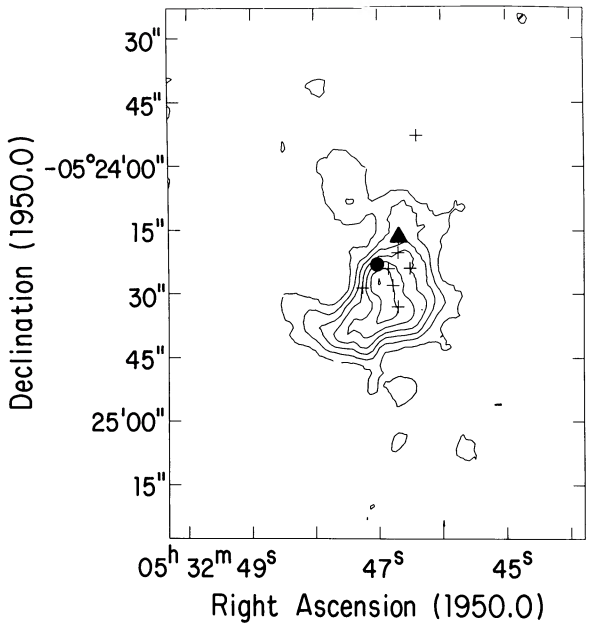

FIG. 1.—Total integrated $2_{11} \rightarrow 2_{12}$ H_2CO emission. Contours are 10, 25, 40, 55, 70, 85, and 100 K km s^{-1}. The positions of the infrared sources IRc1 through IRc9 (Downes *et al.* 1981) are indicated. The filled circle is IRc2 and the filled triangle is IRc1 (the Becklin-Neugebauer object).

width of greater than 13 km s^{-1}. Since the hot core dominates the Barvainis and Wootten map, which covered a much larger velocity range, the present observations probably underestimate the hot core flux owing to emission in velocity channels outside our range. The peak $2_{11} \rightarrow 2_{12}$ hot core brightness temperature is 12.9 K (1 Jy per beam = 5.6×10^{-3} K). We are unable to accurately determine the central velocity of the hot core component because of contamination from the compact ridge emission. However, the hot core emission is clearly confirmed by our high-excitation $4_{23} \rightarrow 3_{22}$, $4_{22} \rightarrow 3_{21}$, $4_{32} \rightarrow 3_{31}$, and $4_{31} \rightarrow 3_{30}$ profiles (see Fig. 7), from which we find that the central velocity of the hot core is near $V_{LSR} = 6.0$ km s^{-1},

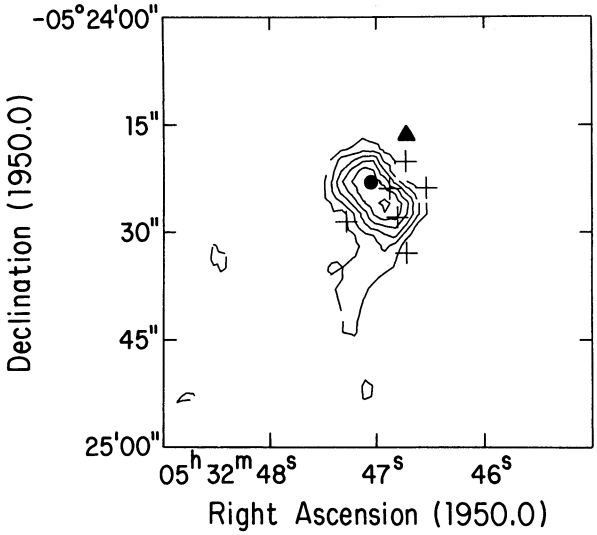

FIG. 2.—$2_{11} \rightarrow 2_{12}$ H_2CO emission integrated over $1 \leq V_{LSR} \leq 6$ km s^{-1}. Contours are 5, 10, 15, 20, 25, and 30 K km s^{-1}. The positions of the infrared sources are as in Fig. 1.

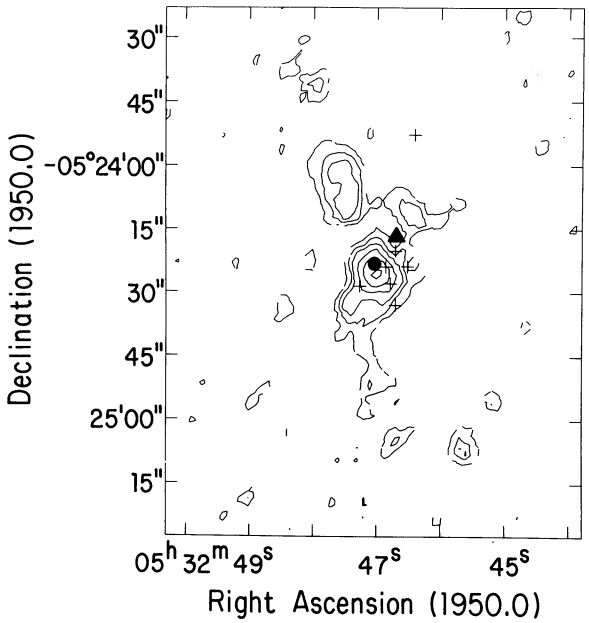

FIG. 3.—$2_{11} \rightarrow 2_{12}$ H_2CO emission integrated over $1 \leq V_{LSR} \leq 6$ km s^{-1} and $10 \leq V_{LSR} \leq 14$ km s^{-1}. The condensation to the NE of the hot core is the 10 km s^{-1} feature. This map is the best representation of the H_2CO hot core. Contours are 5, 10, 15, 25, 35, and 45 K km s^{-1}. The position of the infrared sources are as in Fig. 1.

completely consistent with the 2 cm hot core emission distribution and the hot core velocity as measured by other molecules.

ii) *Plateau*

In Figure 4 we present a position-velocity plot at a position angle of 120° through the location of IRc2. There is evidence for a blueshift to the northwest and a redshift to the southeast

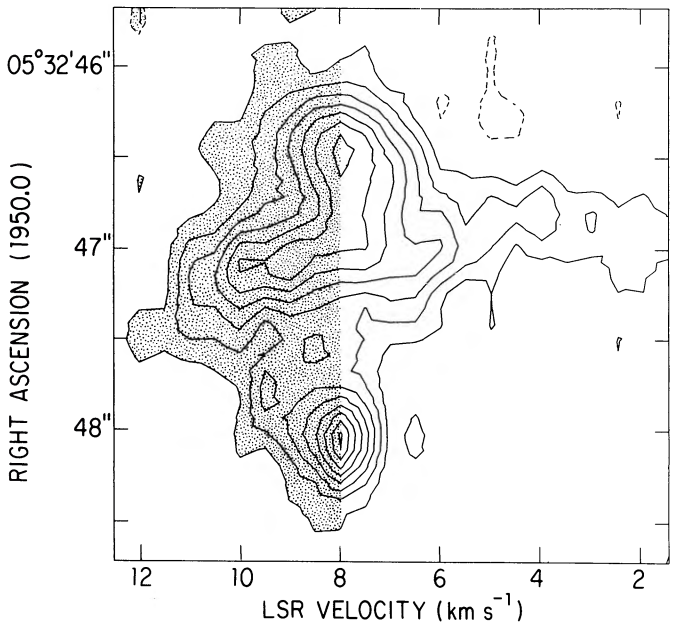

FIG. 4.—Position-velocity plot of the $2_{11} \rightarrow 2_{12}$ H_2CO emission at position angle 120° through the position of IRc2. Relative to 8 km s^{-1}, redshifted emission is shown as the stippled region. Notice the shift from blueshift in the NW to redshift in the SE, in the same sense as that observed in the bipolar flow emanating from IRc2. Contours are −3, 3, 6, 9, 12, 15, 18, 21, and 24 K.

of IRc2 (position-velocity plots at position angles of 90° and 150° do not show this shift). This same velocity shift is also seen in SiO (Wright *et al.* 1983), HCO^+ (Vogel *et al.* 1984), H_2 (Hough *et al.* 1986), SO_2 (Plambeck 1987), and CO (Masson *et al.* 1987) emission, all of which trace the high-velocity plateau or bipolar flow emanating from IRc2. One might expect to see the bipolar flow in our 2 cm emission maps given the high- and low-velocity line wings on millimeter emission line profiles (Figs. 7 and 8; see also Wootten, Loren, and Bally 1984) and in single-antenna profiles of the $2_{11} \rightarrow 2_{12}$ emission line (Vanden Bout 1987; Bastien *et al.* 1985). The detection of H_2CO in the bipolar flow is somewhat surprising since the reactions which most efficiently destroy H_2CO involve O, H, and OH, which are thought to be abundant in a shocked gas (Wootten, Loren, and Bally 1984).

iii) *Compact Ridge*

In Figure 5 we present individual line channel maps of the 2 cm H_2CO emission which comprises the compact ridge. The rms noise in each of these maps is 1.6 K. Figure 6 is the H_2CO compact ridge integrated intensity map ($6 < V_{LSR} < 10$ km s^{-1}). The bulk of the integrated emission over the limited velocity range of our data comes from this component, which in our maps has a peak brightness temperature of 39.4 K, is centered at $V_{LSR} = 8.0$ km s^{-1}, and has a FWZI of ~ 5 km s^{-1}. This center velocity, FWZI, and position of the H_2CO compact ridge are in excellent agreement with, for example, the HDO and CH_3OH compact ridge emission mapped by Plambeck and Wright (1987) and Plambeck and Wright (1988), respectively.

By fitting a Gaussian model to this component, we have found that the H_2CO compact ridge peak lies within 2″ of the position, measured by Churchwell *et al.* (1987), of a compact 2 cm continuum source (Churchwell *et al.* designated it source H). Garay (1987) has also detected this source at 5 and 15 GHz and points out that it exhibits a flat radio spectrum, a characteristic indicative of optically thin, thermal emission. Garay also points out that in order to produce the observed radio flux densities, a Lyman continuum flux of $\simeq 5 \times 10^{43}$ photons s^{-1} is required. This flux can be provided by a B3 ZAMS star (Panagia 1973). Churchwell *et al.* suggest that this source is internally ionized (given its projected location near the core of the Orion-KL nebula) with a structure similar to that of the Becklin and Neugebauer (BN) object (IRc1). Since our H_2CO observations trace the densest gas in the Orion-KL region, and given the spatial coincidence with the radio continuum object listed above, we suggest that the early stages of the star formation process are occuring in the compact ridge.

iv) 10 km s^{-1} *Feature*

In Figures 3 and 5 there is an individual feature in our H_2CO maps situated to the northeast of the hot core and compact ridge. Given its $V_{LSR} = 10$ km s^{-1} and FWZI ~ 1.5 km s^{-1}, we identify this feature with the 10 km s^{-1} feature seen also in CS (Mundy *et al.* 1988), NH_3 (Genzel *et al.* 1982), ^{13}CO (Masson *et al.* 1987), HC_3N (Masson and Mundy 1988) and 3 mm continuum emission maps (it corresponds to the continuum source CS1 of Mundy *et al.* 1986). The existence of a "quiescent ridge" running northeast–southwest with $\Delta V \simeq 4$ km s^{-1} and $V_{LSR} \simeq 9$ km s^{-1} has led to the suggestions that this 10 km s^{-1} feature is either (*a*) an individual cloud, not associated with the more dominant 8 km s^{-1} feature on this ridge (Bastien *et al.* 1985; Ho and Barrett 1978) or (*b*) the result

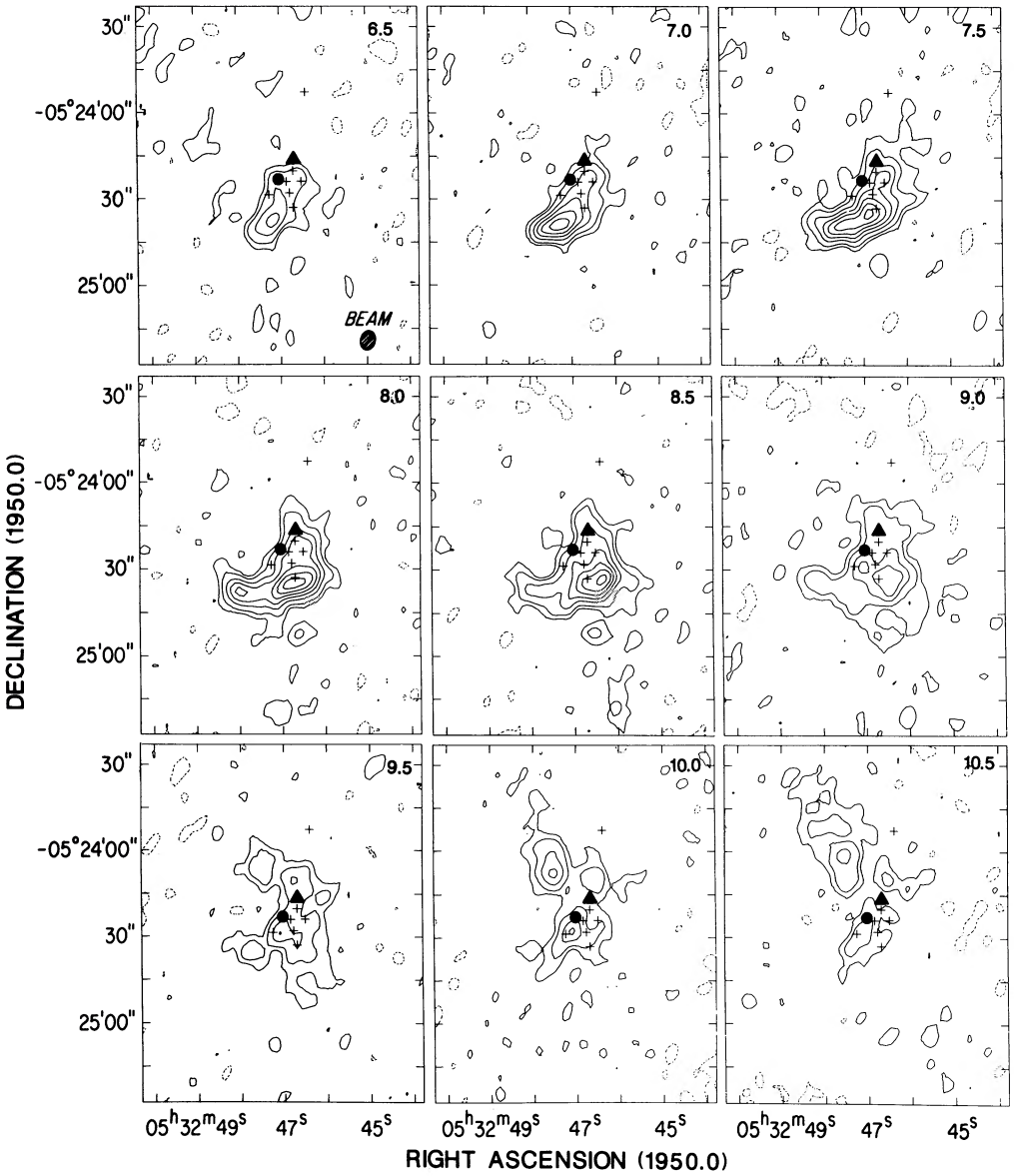

FIG. 5.—Maps of the $2_{11} \rightarrow 2_{12}$ H_2CO emission from the compact ridge and 10 m s^{-1} feature. The contours are −3, 3, 6, 12, 18, 24, 30, and 36 K. The central LSR velocity is given in the upper right-hand corner of each map. The positions of the infrared sources are as in Fig. 1.

of differential rotation of a nearly edge-on disk in the ridge (Liszt *et al.* 1974; Vogel *et al.* 1985). The 2 cm H_2CO emission tends to trace the higher density gas (2 cm H_2CO emission requires $n(H_2) \geq 10^6$ cm^{-3}). Ho and Barrett based their conclusion on observations of the $(J, K) = (2,2)$ line of NH_3, a transition also sensitive to high densities. Given that the two-cloud model is based upon observations sensitive only to high densities while the edge-on rotating disk model in based upon observations of the lower density tracing molecules CO (Liszt *et al.*) and HCN (Vogel *et al.*), we favor an interpretation in which the quiescent ridge, consisting of dense clumps of gas and dust, lies embedded in a less dense medium which is differentially rotating (though our observations do not show this rotation).

We have also searched for internal rotation of the 10 km s^{-1} feature by looking for a velocity gradient across this component. We find no evidence for rotation, but cannot rule out the existence of velocity gradients smaller than our velocity resolution of 0.5 km s^{-1}. This upper limit to the rotation velocity of the 10 km s^{-1} feature implies an angular velocity of $\leq 10^{-13}$ rad s^{-1} (assuming a source size given by a Gaussian fit to the H_2CO 10 km s^{-1} feature; see Table 1). Observed disk rotational velocities in other sources exceed this limit (Wootten 1985).

b) Single Antenna

Single antenna profiles of H_2CO, $H_2{}^{13}CO$, and $H_2C^{18}O$ are shown in Figures 7 through 10. In Figure 7 we display the H_2CO transitions observed prior to 1987 December. Figure 8 shows our new submillimeter H_2CO detections. Figures 9 and 10 show our $H_2{}^{13}CO$ and $H_2C^{18}O$ detections, respectively. Line parameters, as determined from Gaussian fits to these profiles, are given in Tables 2 and 3. As can be seen from Table 2, many of the H_2CO transitions observed show a multiple-

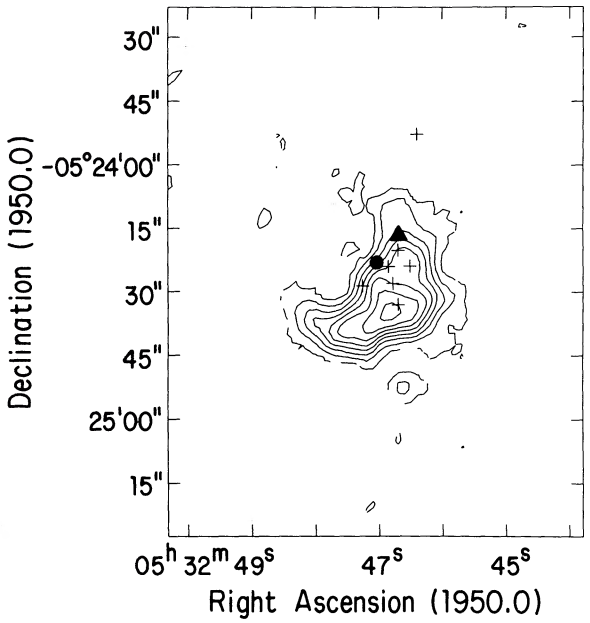

FIG. 6.—The integrated $2_{11} \rightarrow 2_{12}$ H_2CO emission over the velocity range $6 < V_{LSR} < 10$ km s^{-1}, representative of the compact ridge. Contours are 5, 15, 25, 35, 45, 55, 65, and 78 K km s^{-1}. The positions of the infrared sources are as in Fig. 1.

component structure. The dominant component in all cases originates from the compact ridge. Note also that the transitions involving the highest energy levels clearly demonstrate the presence of the hot core component in the low velocity wings.

Two of the observed $H_2C^{18}O$ transitions suffer from possible contamination. The $3_{12} \rightarrow 2_{11}$ transition at 214.778490 GHz is blended with an unidentified line in the signal sideband at ~214.783 GHz. The other potentially contaminated spectrum, the $H_2C^{18}O$ $4_{14} \rightarrow 3_{13}$ transition, appears to be abnormally strong in comparison to the other two $H_2C^{18}O$ transitions detected. We believe this to be due to contamination from CH_3OH $9_{-5} \rightarrow 10_{-4}$ at 268.744050 GHz.

Figures 11 and 12 show maps of the H_2CO $4_{14} \rightarrow 3_{13}$, $4_{13} \rightarrow 3_{12}$, and $H_2{}^{13}CO$ $3_{12} \rightarrow 2_{11}$ transitions. The map of the 300.836635 GHz $4_{13} \rightarrow 3_{12}$ transition (Fig. 12) is the first submillimeter H_2CO map made of this region and clearly delineates the Orion-KL ridge. The structure observed is similar to that seen in other spectral line maps of the Orion-KL ridge. The condensation 2′ south of the hot core/compact ridge region does not show up on our 2 cm maps because it is situated beyond the half-power point of our 2 cm VLA beam. The peak of the $4_{13} \rightarrow 3_{12}$ H_2CO emission in this map occurs at a position and velocity characteristic of the compact ridge. The FWHM size of this region is 80″ in declination and ≤20″

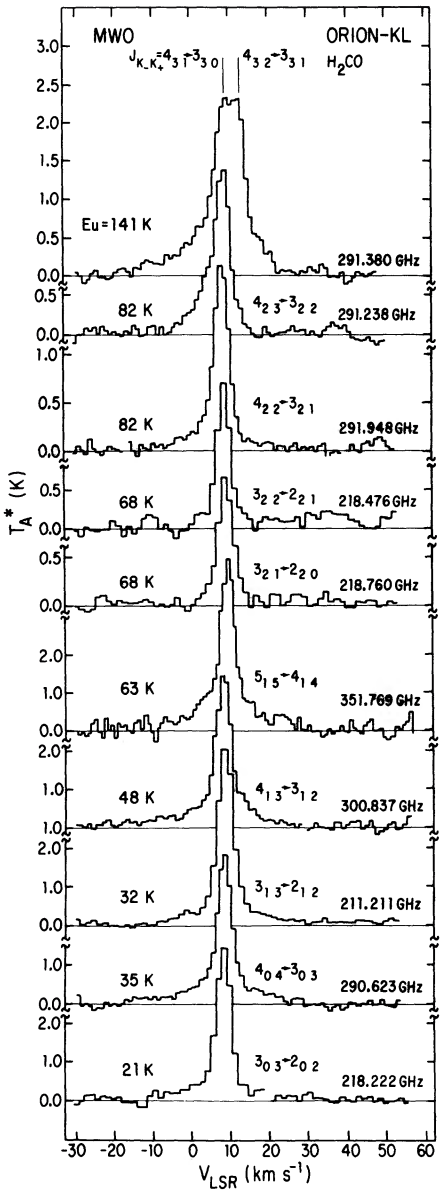

FIG. 7.—Single antenna profiles of H_2CO emission in Orion-KL. The pointing center position is $\alpha(1950) = 05^h32^m46^s.7$, $\delta(1950) = -05°24'25''$. The velocity resolution in these spectra ranges from 0.9 km s^{-1} at 351.769 GHz to 1.4 km s^{-1} at 211.211 GHz. For each spectrum the transition, upper state energy above the ground state, and frequency are indicated. All spectra were obtained prior to the telescope upgrade.

in right ascension. Due to the fact that gas at densities below $\sim 10^6$ cm^{-3} does not produce 2 cm H_2CO emission, we believe that the source size derived from this $4_{13} \rightarrow 3_{12}$ H_2CO emis-

TABLE 1

2 cm H_2CO CONDENSATION CHARACTERISTICS

Component	α(1950)	δ(1950)	Angular Size (arcsec)	Peak T_B (K)	FWZI (km s^{-1})	$\int T_B dv$ (K km s^{-1})	$N(H_2CO)$ (cm^{-2})
Hot core	$05^h32^m47^s.0$	−05°24′26″	10.7 × 9.2	12.9	>13.0[a]	>46.74[a]	$>1.1 \times 10^{17}$[a]
Compact ridge	05 32 46.9	−05 24 33	27.1 × 15.8	39.4	5.0	74.81	4.1×10^{16}
10 km s^{-1} feature	05 32 47.5	−05 24 05	17.4 × 9.3	19.5	1.5	26.42	7.6×10^{15}

[a] Lower limit due to extension of emission below 1.0 km s^{-1}.

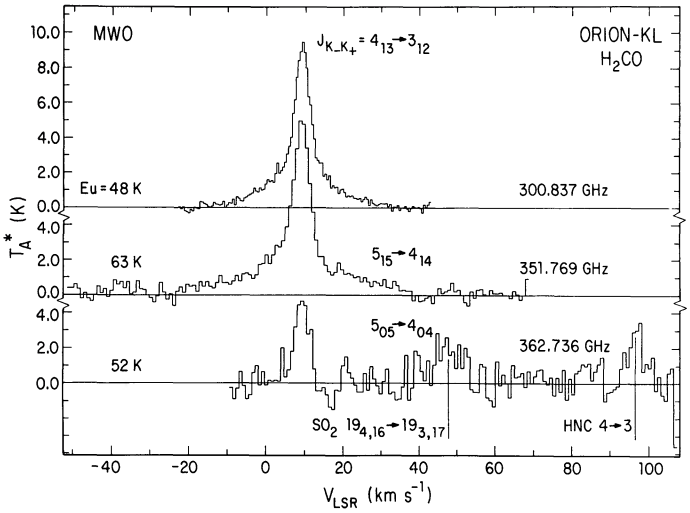

FIG. 8.—Single-antenna submillimeter profiles of H_2CO emission in Orion-KL. The pointing center and annotation for each spectrum are the same as that in Fig. 7. The velocity resolution is 0.3 km s^{-1} at 300.837 GHz, 0.9 km s^{-1} at 351.769 GHz, and 0.8 km s^{-1} at 362.736 GHz. All spectra were obtained after the telescope upgrade. In the $5_{05} \rightarrow 4_{04}$ spectrum an SO_2 line from the image sideband at 359.771 GHz and an HNC line at 362.630 GHz are indicated.

sion map represents our best estimate of the physical size of the H_2CO compact ridge.

IV. DISCUSSION

A key question we wish to address is: What variation does the H_2CO abundance show among the various components comprising the Orion-KL core? In § IV*a* below we discuss the H_2CO column density based on the interferometric maps alone. These are sensitive to variations on small spatial scales but a detailed interpretation must rely on global excitation characteristics determined over larger scales by single antennas. In § IV*b* we discuss non–LTE models of the large-scale emission, which accurately constrain the excitation conditions and accurately measure column densities, including extended low-level emission (densities $\lesssim 10^6$ cm^{-3} to which the emission in the $2_{11} \rightarrow 2_{12}$ transition is not sensitive). These measurements cannot of course accurately track variations over small spatial scales. For instance, the 10 km s^{-1} feature cannot be independently modeled on the basis of any of our single-antenna data. However, note that the strength of the line emission increases sharply at the hot core/compact ridge position observed in the interferometer maps. Therefore, the hot core/compact ridge contribution dominates the observed single antenna profiles also. Combination of the two data sets provides a very accurate measure of the H_2CO emission in Orion-KL and its abundance in the various components of that emission. Finally, in § IV*c* we compare the abundance of H_2CO with that of other common molecules.

a) Individual Component Formaldehyde Column Densities

Below we calculate the H_2CO column densities for the hot core, compact ridge, and 10 km s^{-1} feature using our interferometer observations. In § IV*b* we use our multi-transition, multi-isotopomer data set to calculate the $H_2{}^{13}CO$ and $H_2C^{18}O$ column densities in the compact ridge. Given our results from § III*b*, we estimate the geometric mean size of the H_2CO compact ridge to be $\sim 40''$. Therefore, our derived single antenna column densities will give a good measure of the compact ridge column density when corrected for optical depth and a beam filling factor of $(40''/60'')^2 = 4/9$.

To calculate the total H_2CO column density as measured by our interferometer observations, we assume that the $2_{11} \rightarrow 2_{12}$ transition is optically thin and that the rotational temperature which describes the population of the H_2CO levels is the kinetic temperature of the gas. In order to check this first assumption, we have compared single-antenna observations of 2 cm H_2CO emission (Bastien *et al.* 1985; Vanden Bout 1987) with those of 2 cm $H_2{}^{13}CO$ emission (Bastien *et al.* 1985; Rood 1988). By assuming the $H_2{}^{13}CO$ transition to be optically thin,

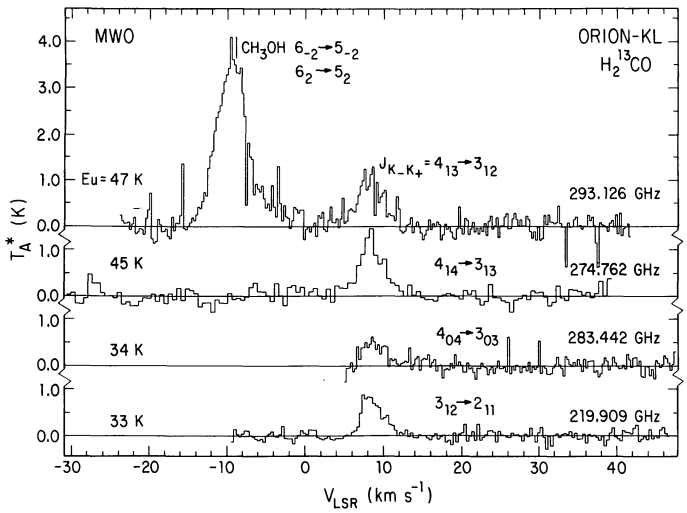

FIG. 9.—Single antenna profiles of $H_2{}^{13}CO$ emission in Orion-KL. The pointing center and annotation for each spectrum are the same as that in Fig. 7. The velocity resolution in these spectra is 0.3 km s^{-1}. In the $4_{13} \rightarrow 3_{12}$ spectrum a CH_3OH line from the image sideband at 290.380 GHz is indicated.

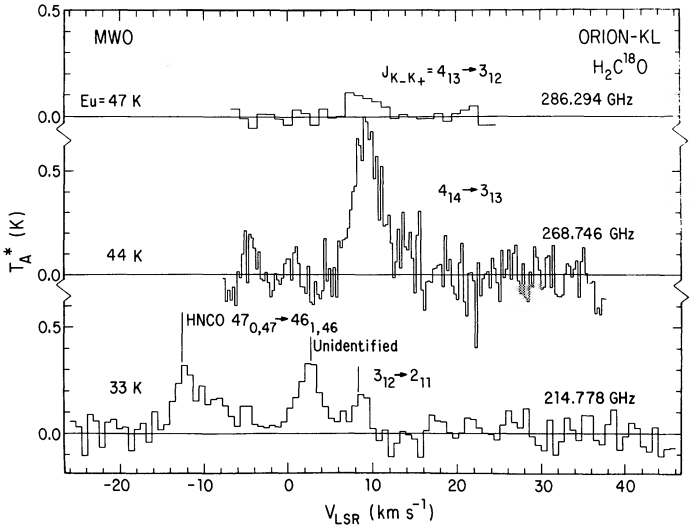

FIG. 10.—Single-antenna profiles of $H_2C^{18}O$ emission in Orion-KL. The pointing center and annotation for each spectrum are the same as that in Fig. 7. The velocity resolution in the 286.294 GHz spectrum is 1.0 km s^{-1}, while in the 268.746 and 214.778 GHz spectra it is 0.3 km s^{-1}. The anomalously large antenna temperature observed in the 268.746 GHz spectrum is probably due to contamination from CH_3OH $9_{-5} \rightarrow 10_{-4}$ at 268.744 GHz. In the $3_{12} \rightarrow 2_{11}$ spectrum an HNCO line at 214.791 GHz and an unidentified line at $\sim$214.783 GHz are indicated.

TABLE 2

SINGLE ANTENNA H_2CO OBSERVATIONS

			Hot Core/Plateau[a]			Compact Ridge			
Frequency (GHz)	Transition	E_u (K)	T_A^* (K)	V_{LSR}[b] (km s^{-1})	FWHM[c] (km s^{-1})	T_A^* (K)	V_{LSR} (km s^{-1})	FWHM (km s^{-1})	Date[d]
291.380452	$4_{32} \rightarrow 3_{31}$	141.1	blend	blend	blend	1.2 ± 0.1	9.0 ± 1.0	3.7 ± 1.0	1983 Dec
			...	...	...	2.4 ± 0.5	9.0 ± 1.0	3.7 ± 1.0	1988 Jan
291.384371	$4_{31} \rightarrow 3_{30}$	141.1	0.3 ± 0.1	6.0 ± 1.0	17.9 ± 1.0	1.2 ± 0.1	9.0 ± 1.0	3.7 ± 1.0	1983 Dec
			...	...	...	2.4 ± 0.5	9.0 ± 1.0	3.7 ± 1.0	1988 Jan
291.237770	$4_{23} \rightarrow 3_{22}$	82.2	0.7 ± 0.1	6.1 ± 1.0	11.0 ± 1.0	1.6 ± 0.1	9.0 ± 1.0	3.7 ± 1.0	1983 Dec
			...	...	...	2.4 ± 0.5	9.8 ± 0.5	3.9 ± 1.3	1988 Jan
291.948072	$4_{22} \rightarrow 3_{21}$	82.2	0.3 ± 0.1	6.6 ± 1.0	16.9 ± 1.0	1.6 ± 0.1	8.5 ± 1.0	4.0 ± 1.0	1984 Feb
			...	...	...	3.1 ± 0.4	9.7 ± 0.2	3.4 ± 0.4	1988 Jan
218.475639	$3_{22} \rightarrow 2_{21}$	68.2	...	...	...	1.8 ± 0.1	8.2 ± 1.0	4.3 ± 1.0	1984 May
			...	...	...	2.6 ± 0.8	8.5 ± 0.5	4.0 ± 1.2	1988 Jan
218.760068	$3_{21} \rightarrow 2_{20}$	68.2	...	...	...	1.5 ± 0.1	8.7 ± 1.0	5.2 ± 1.0	1983 May
			...	...	...	2.9 ± 0.4	8.6 ± 0.2	4.5 ± 0.6	1988 Jan
351.768639	$5_{15} \rightarrow 4_{14}$	62.5	1.0 ± 0.2	9.0 ± 1.0	20.1 ± 1.0	3.5 ± 0.2	9.4 ± 1.0	3.7 ± 1.0	1985 Feb
			2.2 ± 0.1	8.1 ± 0.3	30.6 ± 0.3	7.4 ± 0.1	9.0 ± 0.3	5.1 ± 0.3	1988 Feb
362.735920	$5_{05} \rightarrow 4_{04}$	52.4	...	...	...	4.7 ± 0.1	9.3 ± 0.3	4.5 ± 0.3	1988 Feb
300.836635	$4_{13} \rightarrow 3_{12}$	47.9	0.6 ± 0.1	7.1 ± 0.3	22.3 ± 0.8	3.3 ± 0.1	8.8 ± 0.1	4.3 ± 0.2	1984 Feb
			2.6 ± 0.2	8.3 ± 0.3	18.2 ± 0.8	6.2 ± 0.2	9.1 ± 0.1	4.5 ± 0.2	1988 Jan
281.526949	$4_{14} \rightarrow 3_{13}$	45.6	1.2 ± 0.5	7.2 ± 1.0	21.2 ± 1.0	6.2 ± 0.5	9.4 ± 1.0	3.8 ± 1.0	1982 Feb[e]
			2.3 ± 0.1	8.3 ± 0.2	20.1 ± 0.6	8.4 ± 0.1	9.0 ± 0.1	4.3 ± 0.1	1987 Dec
290.623416	$4_{04} \rightarrow 3_{03}$	34.9	0.6 ± 0.1	7.4 ± 1.0	21.3 ± 1.0	3.2 ± 0.1	8.9 ± 1.0	4.1 ± 1.0	1984 Feb
225.697760	$3_{12} \rightarrow 2_{11}$	33.5	0.8 ± 0.1	7.8 ± 1.0	20.6 ± 1.0	4.2 ± 0.1	9.0 ± 1.0	4.2 ± 1.0	1982 May[e]
			1.5 ± 0.6	8.2 ± 1.6	16.8 ± 5.9	7.7 ± 0.6	8.8 ± 0.2	4.1 ± 0.5	1988 Jan
211.211469	$3_{13} \rightarrow 2_{12}$	32.1	0.5 ± 0.1	8.5 ± 1.0	19.9 ± 1.0	4.0 ± 0.1	8.5 ± 1.0	4.4 ± 1.0	1983 May[e]
218.222191	$3_{03} \rightarrow 2_{02}$	21.0	...	...	...	3.5 ± 0.1	8.6 ± 1.0	4.1 ± 1.0	1984 Feb
			...	...	...	4.3 ± 0.4	8.6 ± 0.2	4.2 ± 0.4	1988 Jan

[a] Signal-to-noise not sufficient to detect plateau in some scans.
[b] Hot core has $V_{LSR} \simeq 6$ km s^{-1} while the plateau has $V_{LSR} \simeq 7$–8 km s^{-1}.
[c] Due to the weakness of these transitions in the hot core and plateau, FWHM derived from Gaussian deconvolution should be treated only as a rough estimate of the true line width.
[d] System was approximately twice as efficient for 1987 Dec and 1988 Jan and Feb observations.
[e] Published in Wootten, Loren, and Bally 1984.

we conclude that $\tau < 1$ in the $2_{11} \rightarrow 2_{12}$ transition of H_2CO (our model results also confirm this assumption; see § IV*b* below). Given these assumptions, the total H_2CO column density is given by

$$N(H_2CO) = \frac{3kQ_{ROT}}{8\pi^3 \nu \mu^2 g_I S_{ij}} \exp\left(\frac{E_u}{kT_K}\right) \int T_B \, dv \times 10^5 \text{ cm}^{-2}$$

where dv is in km s^{-1}, the spin degeneracy $g_I = \frac{3}{4}$ for ortho-H_2CO, $\mu = 2.331$ debye, and for the 2 cm transition the line strength $S_{ij} = 0.833$, $E_u/k = 22.63$ K, and $Q_{ROT} = 0.138 T_K^{3/2}$. The temperature of the hot core and compact ridge has been measured by Loren and Mundy (1984) using a multi-transition study of methyl cyanide (CH_3CN). They find that $T_K = 275 \pm 25$ K for the hot core and $T_K = 95 \pm 8$ K for the compact ridge, in good agreement with less accurate determinations from H_2CO lines alone derived in the next section. Using the integrated intensities calculated from the Gaussian fits to Figures 3 and 6 (see Table 1), we find that $N(H_2CO) > 1.1 \times 10^{17}$ cm^{-2} for the hot core (lower limit due to extension

TABLE 3

$H_2{}^{13}CO$ AND $H_2C^{18}O$ OBSERVATIONS

Isotopomer	Frequency (GHz)	Transition	E_u (K)	T_A^* (K)	V_{LSR} (km s^{-1})	FWHM (km s^{-1})	Date
$H_2{}^{13}CO$	284.117450	$4_{32} \rightarrow 3_{31}$	140.6	rms = 0.1	...	...	1988 Jan
	284.120620	$4_{31} \rightarrow 3_{30}$	140.6	rms = 0.1	...	...	1988 Jan
	283.992510	$4_{23} \rightarrow 3_{22}$	81.4	rms = 0.1	...	...	1988 Jan
	213.293630	$3_{21} \rightarrow 2_{20}$	67.8	rms = 0.2	...	...	1988 Jan
	293.126370	$4_{13} \rightarrow 3_{12}$	47.0	1.0 ± 0.3	8.2 ± 0.4	4.0 ± 1.0	1988 Jan
	274.762121	$4_{14} \rightarrow 3_{13}$	44.8	1.2 ± 0.2	8.4 ± 0.2	3.6 ± 0.5	1987 Dec
	283.441876	$4_{04} \rightarrow 3_{03}$	34.1	0.5 ± 0.1	8.1 ± 0.5	3.5 ± 1.2	1988 Jan
	219.908510	$3_{12} \rightarrow 2_{11}$	33.0	0.9 ± 0.1[a]	8.5 ± 0.2	3.3 ± 0.4	1988 Jan
$H_2C^{18}O$	277.562780	$4_{23} \rightarrow 3_{22}$	81.4	rms = 0.2	...	...	1987 Dec
	286.293960	$4_{13} \rightarrow 3_{12}$	47.0	0.10 ± 0.02	8.9 ± 0.8	4.0 ± 1.9	1988 Jan
	268.745769	$4_{14} \rightarrow 3_{13}$	44.8	0.64 ± 0.11[b]	9.4 ± 0.2	3.3 ± 0.5	1988 Jan
	214.778490	$3_{12} \rightarrow 2_{11}$	33.0	0.19 ± 0.08	8.7 ± 0.4	1.7 ± 1.0	1988 Jan

[a] Possible contribution due to 10 km s^{-1} feature.
[b] Blended with CH_3OH $9_{-5} \rightarrow 10_{-4}$ at 268.744 GHz.

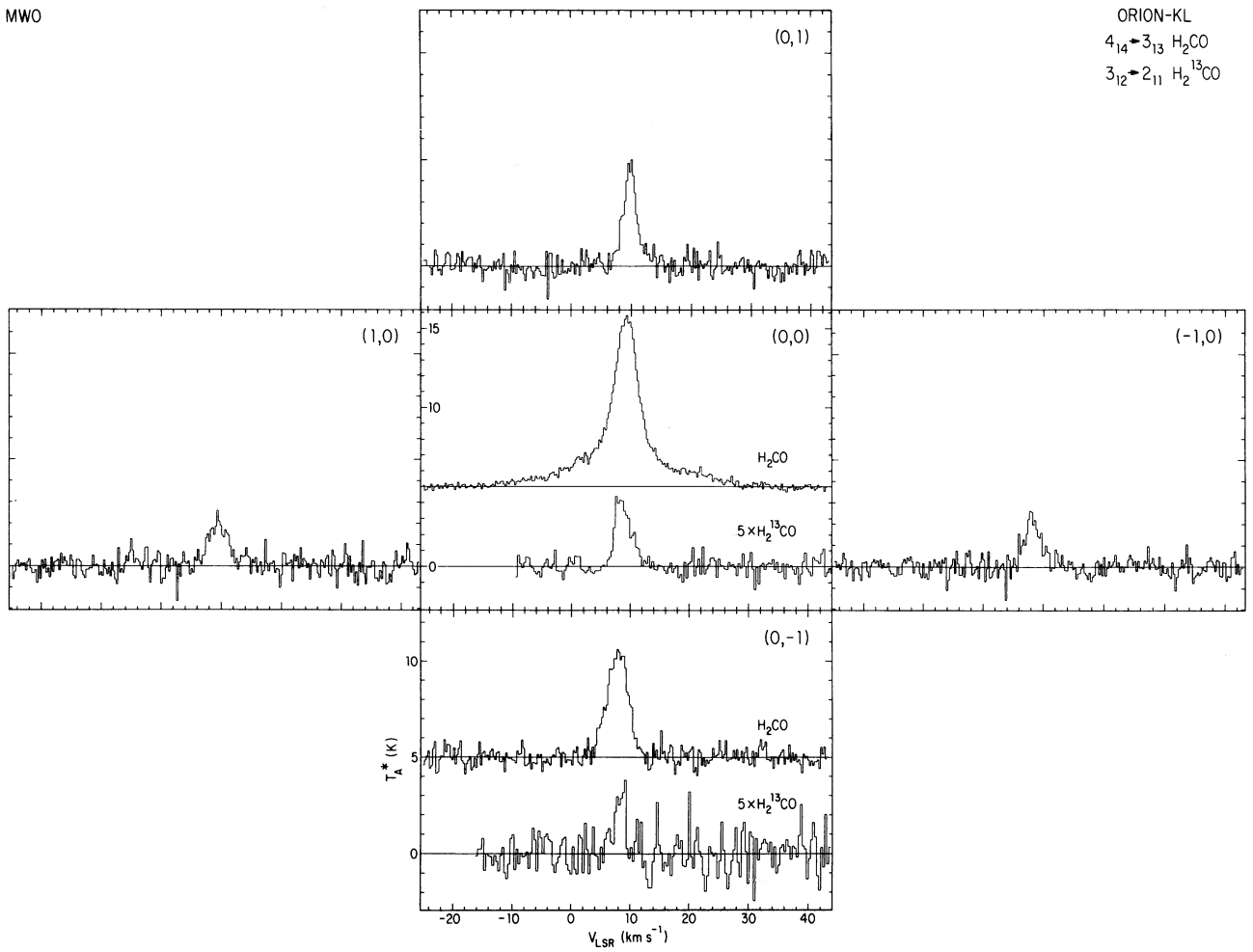

FIG. 11.—Single-antenna map of the $4_{14} \rightarrow 3_{13}$ transition of H_2CO and the $3_{12} \rightarrow 2_{11}$ transition of $H_2{}^{13}CO$ in Orion-KL. The (0,0) position is the same as Fig. 7. Position offsets are given in arcminutes. $H_2{}^{13}CO$ spectra are shown only for two positions. At the (1, 0), (0, 1), and (−1, 0) positions the $H_2{}^{13}CO$ transition was not detected to rms levels of 0.2, 0.3, and 0.5 K, respectively.

of emission below 1.0 km s^{-1}) and $N(H_2CO) = 4.1 \times 10^{16}$ cm^{-2} for the compact ridge. To calculate $N(H_2CO)$ for the 10 km s^{-1} feature, we assume a kinetic temperature, as determined by dust continuum measurements (Werner *et al.* 1976) and a multitransition analysis of CH_3CN (Plambek 1987), of 55 K. Using the integrated intensity determined from a Gaussian fit to this component yields $N(H_2CO) = 7.6 \times 10^{15}$ cm^{-2}.

b) Model Calculations and H_2CO *Abundances*

Large velocity gradient (LVG) and microturbulent slab models were constructed which predicted the formaldehyde spectrum of a molecular cloud. New high-temperature ortho-H_2CO excitation rates calculated by Green (1988) were used in these models, which have enabled us to model the warm gas of the compact ridge and hot core. These models included transitions up to $J = 12$, $E_u/k = 280$ K in the $K = 1$ ladder and $J = 10$, $E_u/k = 290$ K in the $K = 3$ ladder, including all observed lines. The model spectra were matched to the observed multitransition, multi-isotopomer spectrum of the central region of Orion-KL. The ortho-species of each isotopomer was modeled assuming that a compact ridge structure of a single size, temperature, and density gives rise to the emission. Through this process, the temperature of the hot core and compact ridge, and the spatial density and column density of the compact ridge were determined. The first step of the process measured the temperature.

i) *Temperature*

Symmetric top molecules measure kinetic temperature accurately, as the separate rotational ladders interconnect through collisions only, yet transitions in these ladders occur close in frequency and sample a wide range of excitation conditions. The H_2CO molecule is only slightly asymmetric, so observations in its rotational ladders could measure kinetic temperature accurately. The observations in Figure 7 clearly demonstrate the increasing dominance of the hot core in the line profile as excitation of the line increases. The temperature of the two velocity-distinct components has been measured through examination of ratios of profiles in different rotational ladders at the appropriate velocities. A channel-by-channel comparison of the $4_{32} \rightarrow 3_{31}$ to $4_{14} \rightarrow 3_{13}$ profiles shows $R_{K=3/K=1} = 0.13 \pm 0.05$ for the compact ridge, and $R_{K=3/K=1} = 0.25 \pm 0.05$ for the hot core, a ratio which remains constant over a velocity range from $V_{LSR} = -3$ to 6 km s^{-1} (the higher velocity wing is obscured by the blend with the $4_{31} \rightarrow 3_{30}$ line). A similar comparison of the $4_{23} \rightarrow 3_{22}$ to $4_{04} \rightarrow 3_{03}$ transitions of para-H_2CO suggests $R_{K=2/K=0} = 0.76 \pm 0.07$ for the compact ridge, with a marginally different ratio

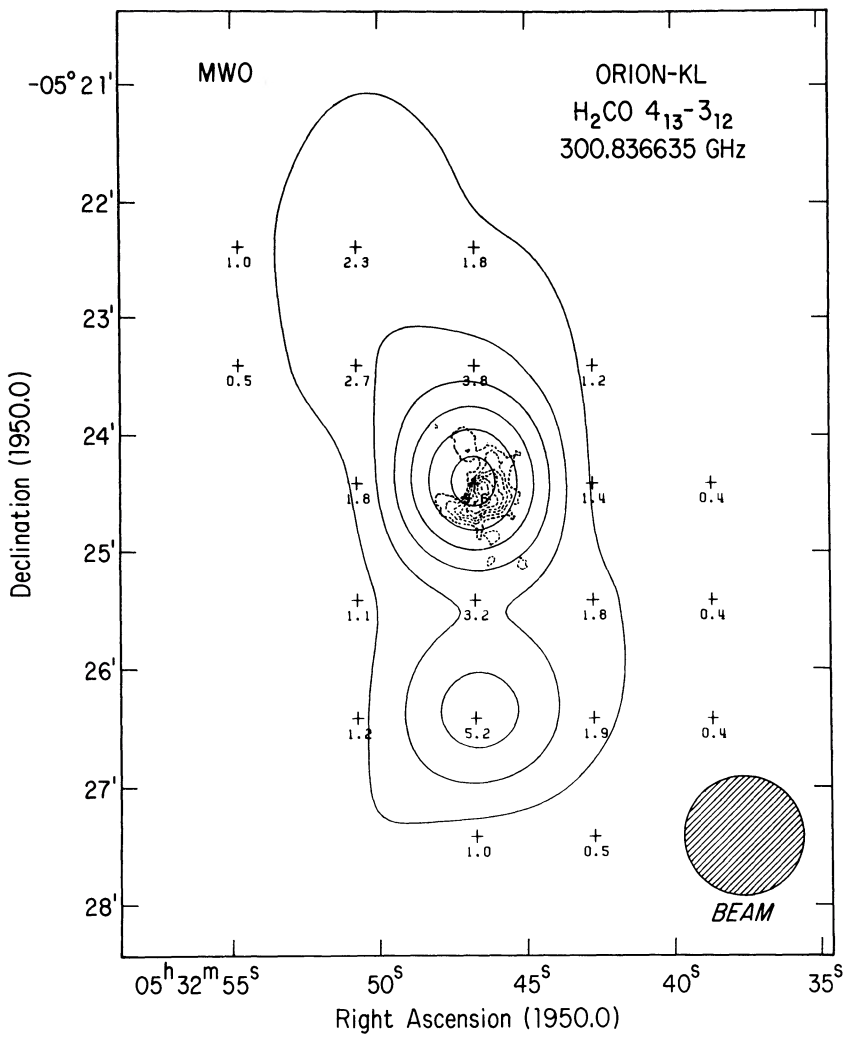

FIG. 12.—Single-antenna map of the $4_{13} \rightarrow 3_{12}$ transition of H_2CO in Orion-KL. Crosses indicate the positions where spectra were obtained, with the observed peak T_A^* given for each position. Contours are 1.5, 3.0, 4.5, 6.0, 7.5, and 9.0 K. The peak T_A^* is 9.6 K. The dashed contours represent the total integrated $2_{11} \rightarrow 2_{12}$ H_2CO emission from Fig. 1. Note that the peak 2' south of the hot core/compact ridge region does not show up on our 2 cm maps because it is situated beyond the half-power point of our 2 cm VLA beam.

of $R_{K=2/K=0} = 0.52 \pm 0.13$ obtaining over velocities characterizing the hot core (V_{LSR} = 5 to 8 km s^{-1}). At their moderate optical depths (see below), the ortho-H_2CO lines suggest T_k(hot core) $\sim 170 \pm 50$ K, consistent with the CH_3CN result cited above. The lower $R_{K=3/K=1} \sim 0.13$ value more characteristic of the compact ridge indicates $T_K \sim 100$ K.

ii) *Density*

As a transition becomes optically thick and thermalized, its intensity loses sensitivity to column density. Even in warm dense optically thin gas, lower excitation transitions do not sensitively measure density. An unwary dependence on model fitting to measure density when low-energy transitions dominate the observations can produce inaccurate density estimates. Line ratios in optically thin lines of differing excitation characteristics respond to density changes in the gas most readily. With several optically thin lines, the partition function, generally not a simple function of temperature, becomes well constrained. Finally, a model may be constructed to fit all of the observations. The first question, then, is what optical depths are characteristic of the observed lines?

As many constraints as possible were derived from the score of measured formaldehyde lines as checks on the models. First the ratios of different isotopic species in corresponding lines were established. These ratios were compared to isotopic abundances measured in other molecular species. From this comparison, approximate optical depths were deduced. This, in turn, yielded estimates of the formaldehyde column density. The models were constrained to match line intensity ratios and strengths for each isotopomer. The final model should provide fits consistent with these and other constraints, and provide the best non–LTE estimates of the density and column density in the compact ridge.

The most secure clue to the optical depths of the lines is obtained from a comparison of H_2CO and $H_2{}^{13}CO$ lines. For all millimeter lines in the $K = 0$ and $K = 1$ ladders, the ratio of corresponding transitions is constant within the errors at 7.2 ± 0.4, suggesting that at least some of the observed transitions are approaching thermalization. In contrast, no $H_2{}^{13}CO$ lines were detected in the $K = 2$ and $K = 3$ ladders with limits $R(H_2CO/H_2{}^{13}CO)_{K=2} > 28$ and $R(H_2CO/H_2{}^{13}CO)_{K=3} > 31$. We conclude that the optical

depths of the H_2CO lines in the $K = 2$ and $K = 3$ ladders lie below that in the millimeter lines in the $K = 0$ and $K = 1$ ladders. However, in the 2 cm transition, the $H_2{}^{13}CO$ transition is more than 40 times weaker than the corresponding H_2CO transition (Bastien *et al.* 1985; Rood 1988), consistent with low optical depth and a $^{12}C/^{13}C$ abundance ratio of 60 (Audouze 1977; Wannier 1980). The moderate peak brightness temperatures found in the VLA maps are consistent with low optical depth in the H_2CO 2 cm line. The millimeter $K = 0$ and 1 H_2CO lines must have appreciable optical depths, while the centimeter and $K = 2$ and 3 lines have lower opacities. The $H_2{}^{13}CO$ lines appear to have optical depths of one at the most, since the centimeter and $K = 2$ and 3 lines must be quite optically thin.

Although the $H_2C^{18}O$ lines are weak, the $H_2{}^{13}CO/H_2C^{18}O$ lines ratios average 2.2 ± 0.4. Excluding the possibly contaminated $4_{14} \rightarrow 3_{13}$ $H_2C^{18}O$ line, the ratio increases to 6 ± 2. This value agrees with the $^{13}C/^{18}O$ ratio measured using other species. The data suggest that the $H_2C^{18}O$ lines are optically thin, supporting the conclusion that the $H_2{}^{13}CO$ lines have moderate optical depth.

By fixing the kinetic temperature in the models at 100 K, we find that the best fit LVG models for ortho-$H_2{}^{13}CO$, -H_2CO, and -$H_2C^{18}O$ in the compact ridge suggest $n(H_2) = 5.0 \times 10^6$ to 1.0×10^7 cm^{-3} [see Table 4 for a comparison between observed and predicted radiation temperatures at $n(H_2) = 5.0 \times 10^6$ cm^{-3}]. Measurements of the $K = 2$ and $K = 3$ lines support this density estimate. Below $n(H_2) \sim 1.0 \times 10^6$ cm^{-3} the $K = 3$ line is quite weak, while by $n(H_2) \sim 5.0 \times 10^7$ cm^{-3} the line rapidly approaches the intensity of the $K = 1$ line as it thermalizes for column densities such as we measure. For the compact ridge, the $R_{K=2/K=0}$ measurement allow $n(H_2) \sim 1.0 \times 10^7$ cm^{-3} at $T_K \sim 100$ K.

In these models, the best fit $H_2{}^{13}CO$ spectrum suggests $N(H_2{}^{13}CO) = (1.1 \pm 0.3) \times 10^{14}$ cm^{-2} and $\tau = 0.1$ to 0.2 in the four millimeter transitions observed. The spectrum of 15 observed H_2CO transitions is best fit by a model with $N(H_2CO) = (3.1 \pm 1.2) \times 10^{15}$ cm^{-2}, $\tau = 1$ to 3 for the observed millimeter transitions, and $\tau = 0.1$ to 0.2 for the $2_{11} \rightarrow 2_{12}$ transition. Within the observational errors, all of the millimeter $K = 1$ lines are saturated, and the $2_{11} \rightarrow 2_{12}$ line strength together with the strength of the K = 3 blend best constrain this column density. The model spectrum indicates that $\Delta J = 0$ transitions provide the best tool for density and column density measurements, as all should be both optically thin and reasonably easily measured. One of these lines lay among the seven transitions from 215 to 263 GHz Blake *et al.* (1987) used to measure $N(H_2CO) = 5.0 \times 10^{15}$ cm^{-2}, contributing to the success of this LTE model. The best fit for the few $H_2C^{18}O$ lines indicates $N(H_2C^{18}O) = (1.0 \pm 0.6) \times 10^{13}$ cm^{-2}, and $\tau \sim 0.05$ in the observed transitions. A ratio of ortho-H_2CO to para-H_2CO of three was determined from our observations, in agreement with previous measurements (Butner 1982), and this ratio has been used to obtain the total H_2CO column densities above.

TABLE 4

LARGE VELOCITY GRADIENT MODEL COMPARISONS WITH OBSERVATIONS[a]

Isotopomer	Transition	Observed T_R (K)	Predicted T_R (K)
H_2CO	[$N(H_2CO) = 3.1 \times 10^{15}$ cm^{-2}]		
	$4_{32} \rightarrow 3_{31}$	14 ± 3	17
	$4_{31} \rightarrow 3_{30}$	14 ± 3	17
	$5_{15} \rightarrow 4_{14}$	44 ± 1	57
	$4_{13} \rightarrow 3_{12}$	37 ± 1	53
	$4_{14} \rightarrow 3_{13}$	49 ± 1	58
	$3_{12} \rightarrow 2_{11}$	45 ± 4	49
	$3_{13} \rightarrow 2_{12}$	67 ± 2	52
$H_2{}^{13}CO$	[$N(H_2{}^{13}CO) = 1.1 \times 10^{14}$ cm^{-2}]		
	$4_{32} \rightarrow 3_{31}$	< 0.6	0.8
	$4_{31} \rightarrow 3_{30}$	< 0.6	0.8
	$4_{13} \rightarrow 3_{12}$	6 ± 2	6
	$4_{14} \rightarrow 3_{13}$	7 ± 1	7
	$3_{12} \rightarrow 2_{11}$	5 ± 1	5
$H_2C^{18}O$	[$N(H_2C^{18}O) = 1.1 \times 10^{13}$ cm^{-2}]		
	$4_{13} \rightarrow 3_{12}$	0.6 ± 0.1	0.6
	$3_{12} \rightarrow 2_{11}$	1.1 ± 0.5	0.5

[a] Model parameters: $n(H_2) = 5.0 \times 10^6$ cm^{-3}, $T_K = 100$ K (compact ridge)

A microturbulent slab model fitted the observed spectra very well for a density of 5.0×10^6 cm^{-3} and a microturbulent broadening parameter of 3.9 km s^{-1}. The column densities which produce the closest match to the observations agree with the LVG models: $N(H_2CO) = 2.3 \times 10^{15}$ cm^{-2}; $N(H_2{}^{13}CO) = 1 \times 10^{14}$ cm^{-2}; $N(H_2C^{18}O) = 1 \times 10^{13}$ cm^{-2}.

The H_2 column density in the compact ridge was measured to be $\sim 1 \times 10^{24}$ cm^{-2} by Keene, Hildebrand, and Whitcomb (1982). Using the source size derived from our interferometer measurements, a normal gas-to-dust ratio, and a distance to the Orion-KL region of between 450 and 500 parsecs, we calculate a density range of 1.5×10^6 to 9.0×10^6 cm^{-3}, in excellent agreement with the formaldehyde models.

iii) *Abundance*

To calculate the H_2CO abundance, $X(H_2CO)$, for the compact ridge, we assume a dust-derived mass of $\sim 50\ M_\odot$ for the Orion-KL region (Keene, Hildebrand, and Whitcomb 1982; Mundy *et al.* 1988). Since the hot core has been estimated to have a mass of $\leq 10\ M_\odot$ (Masson *et al.* 1985; Wright and Vogel 1985), we assume the compact ridge to have a mass of $\sim 40\ M_\odot$. We note also that this mass estimate is consistent with the compact ridge mass calculated assuming a spherical condensation with $n(H_2) = 10^7$ cm^{-3} and a radius of 11″ (a mean radius taken from the Gaussian fits to our 2 cm maps; see Table 1). Using the H_2CO column density of 4.1×10^{16} cm^{-2} derived from our 2 cm results, the average radius of 11″, and a distance of 500 pc, we derive $X(H_2CO) \simeq 3.7 \times 10^{-8}$.

Given the excellent agreement between the models and the observations in our multitransition, multi-isotopomer data set, we believe that the average physical characteristics of the compact ridge are as follows: $n(H_2) = 5.0 \times 10^6$ to 1.0×10^7 cm^{-3}, angular size $\sim 20''$–$40''$, $T_K \sim 100$ K, and $X(H_2CO) \sim 10^{-8}$.

Due to our lack of H_2CO isotopomer information for the hot core and 10 km s^{-1} feature, we use other means to calculate their H_2CO abundances. To calculate the H_2CO abundance in the Orion-KL hot core, we use the H_2CO column density calculated in § IV*a* ($> 1.1 \times 10^{17}$ cm^{-2}) with its measured H_2 column density of 2×10^{24} cm^{-2} (Mundy *et al.* 1986) to calculate $X(H_2CO) \geq 5.5 \times 10^{-8}$. Note that by assuming the hot core to be a spherical condensation with a mass of less than or equal to 10 $M_\odot$, an H_2CO column density of $> 1.1 \times 10^{17}$ cm^{-2}, and a radius of $\sim 2''.5$ (Wright and Vogel 1985; note that this assumed radius is a factor of 2 smaller than that derived from a Gaussian fit to our integrated 2 cm hot core map because of probable contamination from the more extended gas associated with the quiescent molecular ridge) at

a distance of 500 pc, a hot core H_2CO abundance of greater than or equal to 2.0×10^{-8} is obtained. The H_2CO abundance in the 10 km s^{-1} feature can be estimated using the H_2CO column density we calculated in § IV*a* (7.6×10^{15} cm^{-2}) and the H_2 column density measured for the CS1 condensation by Mundy *et al.* (1986) (1.0×10^{24} cm^{-2}), which yields $X(H_2CO) = 7.6 \times 10^{-9}$.

c) Comparison with Other Molecular Distributions

In order to analyze the distribution of the 2 cm H_2CO emission with respect to the distributions observed in other molecules, below we have made a series of comparisons with aperture synthesis maps of Orion-KL in several different molecules. We have also compared the abundances of many of these molecules using their observed column densities. We should point out, though, that due to the different spatial frequency sensitivities of the maps, there may be some loss of flux from extended regions. Hence, the column densities calculated from these observations are only lower limits for the extended regions in Orion-KL. The compact ridge H_2CO abundance, as calculated in § IV*b*, is 10^{-8}.

i) 6 cm H_2CO

We have compared our 2 cm H_2CO maps to the $16'' \times 13''$ resolution aperture synthesis maps of 6 cm H_2CO made by Johnston *et al.* (1983). We find a very good correlation between the two emission distributions, with the peak of the 2 cm compact ridge emission lying coincident with the 6 cm emission peak. The shapes of the two emission regions are also similar, though this correspondence is difficult to make because of the larger beam size used in the 6 cm observations. Johnston *et al.* suggest that the 6 cm emission region does not participate in the outflow and H_2CO must therefore be dissociated by conditions in the high-velocity flow. The lower resolution and lower optical depth in the 6 cm line, though, may have prevented them from being able to detect the flow.

ii) *Dust Continuum*

The $7''.5 \times 7''.1$ aperture synthesis maps of the 95 GHz (3 mm) continuum emission of Orion-KL by Mundy *et al.* (1986) reveal many spatial similarities with the H_2CO emission distributions. The 95 GHz continuum emission from the hot core coincides with the broad H_2CO feature situated $\sim 2''$ south of IRc2. The northeast extension in the continuum emission shows up in our maps as the H_2CO 10 km s^{-1} feature. We have also compared our H_2CO integrated hot core emission map with the 3.4 mm continuum emission maps of Wright and Vogel (1985). These $4''.2 \times 3''.2$ maps show the same spatial distribution as our H_2CO hot core and 10 km s^{-1} feature components. Also, as in the Mundy *et al.* maps, the 3.4 mm continuum and H_2CO hot core and 10 km s^{-1} feature peaks coincide.

The correspondence between the H_2CO hot core and dust continuum emission was also investigated through comparison between the 2 cm H_2CO hot core integrated intensity map and the 2.2–30 μm infrared continuum emission maps of Orion-KL by Wynn-Williams *et al.* (1984). These $2''.0$ to $2''.6$ maps show a hole at the 2 cm H_2CO hot core position in the 20 and 30 μm maps. The hot core column density of 2.0×10^{24} cm^{-2} corresponds to a 3–20 μm dust opacity of greater than 10–50 mag; Wynn-Williams *et al.* suggest that the anticorrelation between hot core and infrared continuum can be partly attributed to extinction by dust associated with the dense material in the hot core.

iii) CS

Comparison with $7''.5$ aperture synthesis maps of the CS $J = 2 \rightarrow 1$ transition (Mundy *et al.* 1986, 1988) shows a very good spatial correlation with the integrated H_2CO hot core emission (Fig. 3). The CS line emission features, which are spatially coincident with the dust continuum features designated by Mundy *et al.* as CS1 and CS2, occupy the same regions as our H_2CO 10 km s^{-1} and hot core/compact ridge features, respectively (poor sensitivity to structures as large as the compact ridge, though, may artificially enhance the sensitivity of the CS observations to the 10 km s^{-1} and hot core features). For the CS1 and CS2 condensations Mundy *et al.* derive minimum CS column densities at peak intensity of 1×10^{15} and 2×10^{16} cm^{-2}, respectively. The CS abundance relative to H_2CO is then greater than 0.13 in the 10 km s^{-1} feature and 0.18 in the hot core. In multitransition surveys of CS and H_2CO, Snell *et al.* (1984) and Mundy *et al.* (1987) found $N(CS)/N(H_2CO) \sim 1.8$ with very little source-to-source variation. The abundance of H_2CO appears to be enhanced in the hot core, then, relative to CS, by an order of magnitude or more.

Densities greater than 10^4 cm^{-3} are required to excite appreciable emission in the CS $J = 2 \rightarrow 1$ transition. Therefore, CS and 2 cm H_2CO emission are probing the densest gas in the cloud core, but the CS emission is optically thick (Mundy *et al.* 1988), so may not optimally trace the regions of highest column density. The apparent underabundance of CS relative to H_2CO may be explained by this fact.

iv) NH_3

The $2''.7$ aperture synthesis maps of NH_3 by Genzel *et al.* (1982) also trace the high-density hot core (these observations were not sensitive to structures greater than or equal to $20''$). H_2CO maps of the hot core (Fig. 3) show a very good spatial coincidence with the NH_3 maps, the peak of the H_2CO emission lying $\sim 2''$ south of the peak of the NH_3 emission. Also, the far northeast component of the $NH_3(4,4)$ emission lies at the same position as the H_2CO 10 km s^{-1} feature in Figures 3 and 5.

The NH_3 transitions observed by Genzel *et al.* were the (4, 4), (4, 2), and (3, 2) inversion lines. They are all very optically thick, but have satellite hyperfine lines which are optically thin. This enabled Genzel *et al.* to use the optically thick central parts of the lines as temperature tracers and the optically thin satellites as tracers of column density. Doing so, Genzel *et al.* derived a peak NH_3 hot core column density of 5×10^{18} cm^{-2} and $T_k = 200$ K. This temperature is characteristic of the hot core, and the measured column density implies a hot core NH_3 abundance relative to H_2CO of less than 45.5. From the NH_3 emission maps of Genzel *et al.*, we estimate the peak $NH_3(4,4)$ brightness temperature in the 10 km s^{-1} feature to be $\sim 20\%$ of that in the hot core component. Correction for the relative velocity half-widths between the 10 km s^{-1} feature and the hot core (the NH_3 hot core spans ~ 10 km s^{-1} while the NH_3 10 km s^{-1} feature probably spans a range similar to that observed in the H_2CO 10 km s^{-1} feature, ~ 1 km s^{-1}) and for the much lower temperature in the 10 km s^{-1} feature (~ 55 K) yields $N(NH_3) \simeq 3 \times 10^{17}$ cm^{-2}. The NH_3 abundance in the 10 km s^{-1} feature, relative to H_2CO, is then 39.5.

The inversion lines observed by Genzel *et al.* require densities greater than 10^6 cm^{-3} to populate the levels collisionally (Morris, Palmer, and Zuckerman 1980; Sweitzer 1978). Since 2 cm H_2CO emission requires densities greater than or equal to

10^6 cm^{-3}, the coincidence between the $NH_3(4,4)$ and H_2CO emission distributions provides further evidence that both of these molecules occupy similar regions in the hot core and 10 km s^{-1} feature.

v) HDO

Plambeck and Wright (1987) have made 3".5 × 3".3 and 5".8 × 4".5 aperture synthesis maps of the $1_{10} \rightarrow 1_{11}$ transition of deuterated water (HDO) which show many similarities to our H_2CO line maps. The bulk of the HDO emission originates from the hot core region, which peaks ~2" south of IRc2. The low-velocity HDO hot core feature at $V_{LSR} < 6$ km s^{-1} coincides exactly with our integrated $V_{LSR} < 6$ km s^{-1} emission (see Fig. 2). They also identify the compact ridge in their $V_{LSR} = 8.0$ km s^{-1} channel map. The correlation between the HDO compact ridge and the H_2CO compact ridge is very good in the velocity range $6 < V_{LSR} < 10$ km s^{-1}. After examination of their 5".8 × 4".5 maps Plambeck and Wright suggest that the compact ridge may be composed of a collection of "streamers" which seem to be connected to the hot core and are directed away from IRc2. The most prominent of these streams lies along the eastern "thumb" of the H_2CO compact ridge emission. Plambeck and Wright suggest that these streamers are formed from ablated material which has been compressed by the outflow from IRc2, which would establish a physical link between the hot core and compact ridge.

For the hot core Plambeck and Wright derive $N(HDO) = 1.0 \times 10^{17}$ cm^{-2}, assuming an excitation temperature of 165 K. For the compact ridge, Plambeck and Wright derive $N(HDO) = 1.3 \times 10^{16}$ cm^{-2} using an excitation temperature of 120 K. Using our assumed hot core and compact ridge excitation temperatures of 275 and 95 K, respectively, raises $N(HDO)$ by a factor of 2 in the hot core and lowers $N(HDO)$ by a factor of 2 in the compact ridge. Using the column densities derived by Plambeck and Wright yields HDO abundances relative to H_2CO of less than 0.91 for the hot core and 0.32 for the compact ridge.

vi) HC_3N

Comparison with the 4" aperture synthesis maps of the $J = 12 \rightarrow 11$ transition of HC_3N by Masson and Mundy (1988) shows good correspondences between the hot core and 10 km s^{-1} feature seen in these maps and our own H_2CO line channel maps (the compact ridge is completely resolved out in the HC_3N maps). This coincidence is not surprising since the 2 cm H_2CO emission and high-J HC_3N emission trace the high-density [$n(H_2) > 10^6$ cm^{-3}] clumps in the Orion-KL region.

From the integrated HC_3N hot core spectrum of Mundy *et al.* we calculate $N(HC_3N) = 8.8 \times 10^{14}$ cm^{-2}. This implies a hot core HC_3N abundance relative to H_2CO of less than 0.008. From the HC_3N channel maps of Mundy *et al.*, assuming the velocity half-width and kinetic temperature in the 10 km s^{-1} feature to be 1 km s^{-1} and 55 K, respectively, we calculate $N(HC_3N) = 8.2 \times 10^{13}$ cm^{-2}. The HC_3N abundance in the 10 km s^{-1} feature, relative to H_2CO, is then 0.011.

vii) H_2O

There is an interesting correspondence between the "low-velocity" H_2O maser positions of Genzel *et al.* (1981) and our integrated H_2CO emission map. Several of these masers seem to cluster near the southwest edge of the H_2CO 10 km s^{-1} feature. The cluster of H_2O masers near IRc4 and 5 are coincident with the peak of the H_2CO compact ridge (see Fig. 13). Plambeck *et al.* (1982) and Vogel *et al.* (1984) have pointed out

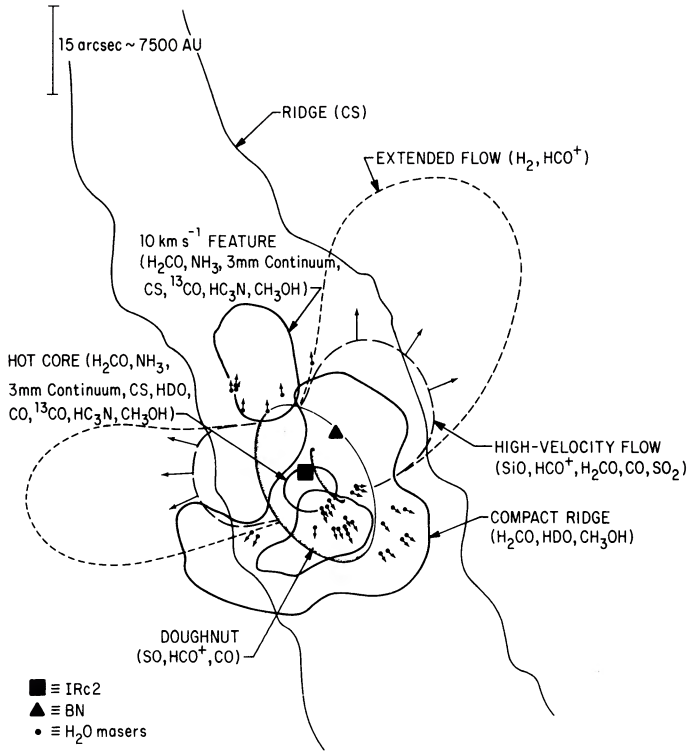

FIG. 13.—The interferometric picture of Orion-KL. With the exception of the extended flow, the molecules and dust continuum used to interferometrically identify each component are indicated. References to these measurements are as follows: H_2CO (this work), NH_3 (Genzel *et al.* 1982), 3 mm continuum (Mundy *et al.* 1986; Wright and Vogel 1985), CS (Mundy *et al.* 1988), HDO (Pambeck and Wright 1987), CO and ^{13}CO (Masson *et al.* 1987), HC_3N (Masson and Mundy 1988), CH_3OH (Plambeck and Wright 1988), SO (Plambeck *et al.* 1982), HCO^+ (Vogel *et al.* 1984), SiO (Wright *et al.* 1983), SO_2 (Plambeck 1987), H_2 (Hough *et al.* 1986), and H_2O (Genzel *et al.* 1981).

that these low-velocity masers sit on the periphery of the expanding "doughnut" of SO and HCO^+ emission centered near IRc2. Genzel *et al.* (1981) have detected proper motion in these masers and have shown that they are moving at velocities less than or equal to 20 km s^{-1}. The measurements indicate a large-scale expansion of the objects from a common centroid somewhere near IRc2. These coincidences suggest that the H_2O maser emission traces regions where the outflow from IRc2 impacts a more massive region, which we see as the compact ridge and 10 km s^{-1} feature.

viii) *Summary*

Figure 13 is a sketch of the Orion-KL region as deduced from these and other interferometric and single antenna observations. In Table 5 we have collected the column densities and relative abundances derived from interferometric observations of some of the molecules discussed above. Two conclusions can be drawn from these comparisons.

1. The H_2CO abundance is virtually the same in the hot core and compact ridge, 5 times lower in the 10 km s^{-1} feature, and 3–5 times lower than the latter over more extended regions in other molecular clouds (Mundy *et al.* 1987; Wootten, Snell, and Evans 1980). Even though many molecular clouds contain high-density regions which can induce 2 cm H_2CO emission, it is seldom observed. The 2 cm emission region in DR 21(OH) was recognized only when high-resolution observations became possible. Therefore, it seems plausible that higher

TABLE 5

COLUMN DENSITY AND ABUNDANCE COMPARISON

Species	Hot Core		Compact Ridge		10 km s^{-1} Feature	
	Column Density (cm^{-2})	Relative Abundance [$N(X)/N(H_2CO)$]	Column Density (cm^{-2})	Relative Abundance [$N(X)/N(H_2CO)$]	Column Density (cm^{-2})	Relative Abundance [$N(X)/N(H_2CO)$]
H_2	2.0×10^{24}	$<6.3 \times 10^6$	1.0×10^{24}	8.3×10^6	1.0×10^{24}	4.5×10^7
H_2CO	$>1.1 \times 10^{17}$	1	4.1×10^{16}	1	7.6×10^{15}	1
CS	$>2.0 \times 10^{16}$	0.18	...	...	$>1.0 \times 10^{15}$	>0.13
NH_3	5.0×10^{18}	<45.5	...	...	3.0×10^{17}	39.5
HDO	1.0×10^{17}	<0.91	1.3×10^{16}	0.32	...	...
HC_3N	8.8×10^{14}	<0.008	...	...	8.2×10^{13}	0.011

resolution observations of other clouds, such as those in the surveys cited above, would uncover regions of 2 cm emission and/or higher H_2CO abundance. It appears then that the high rate of massive star formation (in comparison to, for example, the ρ Oph or DR 21(OH) molecular complexes) in the Orion-KL region has enhanced the H_2CO abundance by releasing these molecules from the surface of icy grain mantles. This progression of enhanced abundance from the 10 km s^{-1} feature to the hot core, in addition to the high density, has defined the region of 2 cm H_2CO emission in Orion-KL.

2. H_2CO, NH_3 (Genzel *et al.* 1982; Hermsen *et al.* 1988), and CH_3OH (Plambeck and Wright 1988) are at least 10 times more abundant in the hot core, compact ridge, and 10 km s^{-1} feature than CS and HC_3N. It has been suggested (Tielens and Allamandola 1987*a*, *b*) that CO, NH_3, CH_3OH, and H_2CO are primary constituents of icy grain mantles in molecular clouds. The sublimation temperatures from grain mantles for these species are in the range 16 to 74 K (Nakagawa 1980). There is also a high degree of deuterium fractionation observed in these molecules toward Orion-KL. For example, $[NH_2D]/[NH_3] = 0.003$ (Walmsley *et al.* 1987), $[HDCO]/[H_2CO] = 0.01$–0.03 (Loren and Wootten 1985), and $[CH_3OD]/[CH_3OH] = 0.01$–0.06 (Mauersberger *et al.* 1988). High deuteration is expected for icy grain mantles formed by grain surface reactions at low temperatures because it is more difficult to abstract deuterium than hydrogen (Tielens and Allamandola 1987*a*, *b*). The high level of deuterium fractionation observed cannot have been produced by very high temperature gas-phase chemical reactions. Consequently, molecules such as CO, NH_3, NH_2D, H_2CO, HDCO, and CH_3OD may have been adsorbed by or produced on grain mantles during an earlier, cooler phase in the evolution of the hot core and compact ridge components. The high densities and temperatures in the hot core and compact ridge, which are more than sufficient to release these molecules, may therefore explain their high abundances in the warm Orion-KL components.

V. CONCLUSIONS

1. The 2 cm hot core emission coincides with that seen in CS, NH_3, HDO, CO, ^{13}CO, HC_3N, CH_3OH, continuum emission peaks at 3 and 3.4 mm and continuum emission holes at 20 and 30 μm (see Fig. 13). The hot core lies $\sim 2''$ south of IRc2. Given its proximity to IRc2, it has been suggested by several authors (Masson and Mundy 1988; Mundy *et al.* 1988) that the hot core may be at least partially bound to IRc2. Using the mass estimate from § IV*b* and assuming a distance to the Orion-KL region of 500 pc and a separation between IRc2 and the hot core of $\sim 2''.5$, we find that the escape velocity for the IRc2/hot core system is ~ 7 km s^{-1}. This is comparable to the observed velocity width of the hot core, which suggests that at least some of the material comprising the hot core can be bound to IRc2. Given the large velocity dispersion and observed ablation of HDO into the compact ridge (Plambeck and Wright 1987), it is also possible that the outflow from IRc2 disrupts the hot core. The H_2CO observations lend some support to this idea. Assuming an age for the outflow from IRc2 of $\sim 10^3$–10^4 yr (Downes *et al.* 1981) and using the angular separation between the hot core and compact ridge of $\sim 7''.6$ ($\simeq 5.7 \times 10^{16}$ cm assuming distance of 500 pc), the compact ridge would need to have a transverse velocity of 1.8–18 km s^{-1} in order to have received ablated material from the hot core. Since the compact ridge is well within the region which participates in the 18 km s^{-1} flow (Genzel *et al.* 1981), it seems plausible from these simple dynamical arguments that some of the hot core material has been pushed down the quiescent ridge into the compact ridge clump.

2. We have detected a bipolar flow in the H_2CO emission in the vicinity of IRc2. The southeast–northwest velocity shift of the H_2CO emission across the position of IRc2 points to a connection with the bipolar flow seen in high-velocity CO, SiO, HCO^+, SO_2, and shocked H_2 emission.

3. The 2 cm H_2CO compact ridge coincides with a similar feature seen in HDO and CH_3OH. Given its central velocity of 8 km s^{-1}, FWZI of ~ 5 km s^{-1}, and apparent connection to the H_2CO hot core emission, we suggest that the compact ridge is a clump in the quiescent molecular ridge which has been compressed by the radial expansion from IRc2. The H_2CO compact ridge is situated on the southern border of the redshifted wing from the bipolar flow (see Fig. 13). This evidence suggests that the compact ridge may have a channeling effect on the southeast portion of the bipolar flow. Since the compact ridge is within the region under the influence of the 18 km s^{-1} flow (Genzel *et al.* 1981), which is thought to have a continuous mass-loss rate of 10^{-3} to 10^{-4} $M_\odot$ yr^{-1} over the 10^3–10^4 yr age of the flow, there has been a total of 10^{-1} to 10 $M_\odot$ of material deposited into the flow. The mass and velocity dispersion in the compact ridge were calculated above to be 40 $M_\odot$ and 5 km s^{-1}, respectively. We invoke conservation of momentum to infer that the compact ridge can indeed affect the direction of the southeast portion of the bipolar outflow.

Given the spatial coincidence with an unidentified compact 2 cm continuum source (Churchwell *et al.* 1987; Garay 1987), the compact ridge may have at its center an internal heat source. Since this object has not been detected at infrared wavelengths, Garay suggests that it could be a heavily enshrouded ZAMS star.

4. The 2 cm H_2CO 10 km s^{-1} feature, which is also seen in

CS, NH_3, ^{13}CO, HC_3N, CH_3OH, and 3 mm continuum emission, lies to the northeast of the hot core, along the quiescent molecular ridge. The 10 km s^{-1} feature is most likely a dense clump in the quiescent molecular ridge. The detection of low-velocity H_2O masers and NH_3 emission on the SW boundary (nearest to the hot core and IRc2) of the 10 km s^{-1} feature supports the notion that this clump may be experiencing a compression from the 18 km s^{-1} outflow emanating from IRc2 (see Fig. 13). In the Plambeck *et al.* (1982) "doughnut" model this feature lies on the northeast edge of the expanding doughnut, again suggesting that the clump has been compressed by the low-velocity outflow.

5. The comparatively high rate of star formation in the Orion-KL region and its effect on icy grain mantles has led to an overabundance of H_2CO, CO, NH_3, and CH_3OH. Coupled with the high degree of deuterium fractionation observed and the suggestion that these molecular species are primarily constituents of icy grain mantles in molecular clouds (Tielens and Alllamandola 1987*a*, *b*), sublimation of these molecules may be the process by which their abundances have been enhanced. We attribute the strength of the 2 cm H_2CO line to the enhancement of the formaldehyde abundance in the active compact ridge region of Orion-KL, as well as to the high densities found there.

6. Lastly, we stress the utility of the spectrum of H_2CO in the 280–300 GHz region as a probe of density, temperature, and formaldehyde abundance. Transitions of two separate rotational ladders of each of the ortho and para subspecies of formaldehyde, a total of seven transitions, lie close in frequency. Calibration and beam size effects are thereby minimized and interpretation of the emission from this light abundant molecule becomes more straightforward.

We thank Shudong Zhou and Harold Butner for making available to us spectra of the $5_{15} \rightarrow 4_{14}$ and $5_{05} \rightarrow 4_{04}$ transitions of H_2CO. We also thank Dick Plambeck and Neal Evans for their helpful and constructive comments which have improved this paper. J. G. M. would like to thank the National Radio Astronomy Observatory for support through their Summer Student Program during the summer of 1987, during which much of the work on this project was completed.

REFERENCES

Audouze, J. 1977, *CNO Isotopes in Astrophysics*, ed. J. Audouze (Dordrecht: Reidel), p. 3.
Barvainis, R., and Wootten, A. 1987, *A.J.*, **93**, 168.
Bastien, P., Batrla, W., Henkel, C., Pauls, T., Walmsley, C. M., and Wilson, T. L. 1985, *Astr. Ap.*, **146**, 86.
Blake, G. A., Sutton, E. C., Masson, C. R., and Phillips, T. G. 1987, *Ap. J.*, **315**, 621.
Butner, H. M. 1982, Senior Thesis, Rensselaer Polytechnic Institute.
Churchwell, E., Felli, M., Wood, D. O. S., and Massi, M. 1987, *Ap. J.*, **321**, 516.
Downes, D., Genzel, R., Becklin, E. E., and Wynn-Williams, C. G. 1981, *Ap. J.*, **244**, 869.
Erickson, N. R. 1981, *IEEE Trans.*, **MTT-29**, 557.
Garay, G. 1987, *Rev. Mex. Astr. Af.*, **14**, 489.
Genzel, R., Downes, D., Ho, P. T. P., and Bieging, J. H. 1982, *Ap. J. (Letters)*, **259**, L103.
Genzel, R., Reidel, M. J., Moran, J. M., and Downes, D. 1981, *Ap. J.*, **244**, 884.
Green, S. 1988, private communication.
Hermsen, W., Wilson, T. L., Walmsley, C. M., and Henkel, C. 1988, *Astr. Ap.*, **201**, 285.
Ho, P. T. P., and Barrett, A. H. 1978, *Ap. J. (Letters)*, **224**, L23.
Hough, J. H., *et al.* 1986, *M.N.R.A.S.*, **222**, 629.
Johansson, L. E. B., *et al.* 1984, *Astr. Ap.*, **130**, 227.
Johnston, K. J., Palmer, P., Wilson, T. L., and Bieging, J. H. 1983, *Ap. J. (Letters)*, **271**, L89.
Keene, J., Hildebrand, R. H., and Whitcomb, S. E. 1982, *Ap. J.*, **252**, L11.
Liszt, H. S., Wilson, R. W., Penzias, A. A., Jefferts, K. B., Wannier, P. G., and Solomon, P. M. 1974, *Ap. J.*, **190**, 557.
Loren, R. B., and Mundy, L. G. 1984, *Ap. J.*, **286**, 232.
Loren, R. B., and Wootten, A. 1985, *Ap. J.*, **299**, 947.
Masson, C. R., Claussen, M. J., Lo, K. Y., Moffet, A. T., Phillips, T. G., Sargent, A. I., Scott, S. L., and Scoville, N. Z. 1985, *Ap. J. (Letters)*, **295**, L47.
Masson, C. R., Lo, K. Y., Phillips, T. G., Sargent, A. I., Scoville, N. Z., and Woodey, D. P. 1987, *Ap. J.*, **319**, 446.
Masson, C. R., and Mundy, L. G. 1988, *Ap. J.*, **324**, 538.
Mauersbeger, R., Henkel, C., Jacq, T., and Walmsley, C. M. 1988, *Astr. Ap.*, **194**, L1.
Morris, M., Palmer, P., and Zuckerman, B. 1980, *Ap. J.*, **237**, 1.
Mundy, L. G. 1981, private communication.
Mundy, L. G., Evans, N. J., II, Snell, R. L., and Goldsmith, P. F. 1987, *Ap. J.*, **318**, 392.
Mundy, L. G., Cornwell, T. J., Masson, C. R., Scoville, N. Z., Bååth, L. B., and Johansson, L. E. B. 1988, *Ap. J.*, **325**, 382.
Mundy, L. G., Scoville, N. Z., Bååth, L. B., Masson, C. R., and Woody, D. P. 1986, *Ap. J. (Letters)*, **304**, L51.
Mundy, L. G., Wootten, A., and Wilking, B. 1989, in preparation.
Nakagawa, N. 1980, in *IAU Symposium 87, Interstellar Molecules*, ed. B. H. Andrew (Dordrecht: Reidel), p. 365.
Olofsson, H. 1984, *Astr. Ap.*, **134**, 36.
Panagia, N. 1973, *A.J.*, **78**, 929.
Plambeck, R. L. 1987, private communication.
Plambeck, R. L., and Wright, M. C. H. 1987, *Ap. J. (Letters)*, **317**, L101.
———. 1988, *Ap. J. (Letters)*, **330**, L61.
Plambeck, R. L., Wright, M. C. H., Welch, W. J., Bieging, J. H., Baud, B., Ho, P. T. P., and Vogel, S. N. 1982, *Ap. J.*, **259**, 617.
Rood, R. T. 1988, private communication.
Snell, R. L., Mundy, L. G., Goldsmith, P. F., Evans, N. J., II, and Erickson, N. R. 1984, *Ap. J.*, **276**, 625.
Sweitzer, J. S. 1978, *Ap. J.*, **225**, 116.
Tielens, A. G. G. M., and Allamandola, L. J. 1987*a*, in *Physical Processes in Interstellar Clouds*, ed. G. E. Morfill and M. Scholer (Dordrecht: Reidel), p. 333.
———. 1987*b*, in *Interstellar Processes*, ed. D. J. Hollenbach and H. A. Thronson, Jr. (Dordrecht: Reidel), p. 397.
Vanden Bout, P. 1987, private communication.
Vogel, S. N., Bieging, J. H., Plambeck, R. L., Welch, W. J., and Wright, M. C. H. 1985, *Ap. J.*, **296**, 600.
Vogel, S. N., Wright, M. C. H., Plambeck, R. L., and Welch, W. J. 1984, *Ap. J.*, **283**, 655.
Wadiak, E. J., Wilson, T. L., Rood, R. T., and Johnston, K. J. 1985, *Ap. J. (Letters)*, **295**, L43.
Walmsley, C. M., Hermsen, W., Henkel, C., Mauersberger, R., and Wilson, T. L. 1987, *Astr. Ap.*, **172**, 31.
Wannier, P. G. 1980, *Ann. Rev. Astr. Ap.*, **18**, 399.
Werner, M. W., Gatley, I., Harper, D. A., Becklin, E. E., Loewenstein, R. F., Telesco, C. M., and Thronson, H. A. 1976, *Ap. J.*, **204**, 420.
Wootten, A. 1985, in *(Sub)millimeter Astronomy*, ed. P. A. Shaver (Munich: ESO), p. 443.
———. 1986, in *IAU Symposium 120, Astrochemistry*, ed. M. S. Vardya and S. P. Tarafdar (Dordrecht: Reidel), p. 311.
Wootten, A., Loren, R. B., and Bally, J. 1984, *Ap. J.*, **277**, 189.
Wootten, A., Snell, R., and Evans, N. J., II. 1980, *Ap. J.*, **240**, 532.
Wright, M. C. H., Plambeck, R. L., Vogel, S. N., Ho, P. T. P., and Welch, W. J. 1983, *Ap. J. (Letters)*, **267**, L41.
Wright, M. C. H., and Vogel, S. N. 1985, *Ap. J. (Letters)*, **297**, L11.
Wynn-Williams, C. G., Genzel, R., Becklin, E. E., and Downes, D. 1984, *Ap. J.*, **281**, 172.

ROBERT B. LOREN: P.O. Box 2915, Silver City, NM 88062

JEFFREY G. MANGUM and ALWYN WOOTTEN: National Radio Astronomy Observatory, Edgemont Rd., Charlottesville, VA 22903

E. JAMES WADIAK: Interferometrics, Incorporated, 8150 Leesburg Pike, Vienna, VA 22180